

INVITED REVIEWS

Gravitational waves from compact objects

José Antonio de Freitas Pacheco

University of Nice-Sophia Antipolis, Observatoire de la Côte d'Azur Laboratoire Cassiopée - UMR
6202 BP 4229 - F606304 - Nice Cedex 4 - France; pacheco@oca.eu

Received 2010 February 14; accepted 2010 July 26

Abstract Large ground-based laser beam interferometers are presently in operation both in the USA (LIGO) and in Europe (VIRGO) and potential sources that might be detected by these instruments are revisited. The present generation of detectors does not have a sensitivity high enough to probe a significant volume of the universe and, consequently, predicted event rates are very low. The planned advanced generation of interferometers will probably be able to detect, for the first time, a gravitational signal. Advanced LIGO and EGO instruments are expected to detect few (some): binary coalescences consisting of either two neutron stars, two black holes or a neutron star and a black hole. In space, the sensitivity of the planned LISA spacecraft constellation will allow the detection of the gravitational signals, even within a “pessimistic” range of possible signals, produced during the capture of compact objects by supermassive black holes, at a rate of a few tens per year.

Key words: gravitational waves — neutron stars — black holes

1 INTRODUCTION

Gravitational waves (GWs) are predicted by General Relativity Theory (GRT) and, after decades of doubts and controversies, the conceptual and mathematical issues of gravitational radiation have presently been clarified. GWs are fundamentally different from electromagnetic waves (EMWs). While the latter propagate in the framework of space and time, the former are waves of the spacetime itself created by asymmetric mass motions. However, they share some properties: both propagate at the same velocity c and linearized GWs have, as EMWs, two independent transverse polarization states (h_+ and h_\times). The field components h_+ and h_\times are derived from double time integrals of the space-time components of the Riemann curvature tensor. They “stretch” and “squeeze” space whereas inertia “stretches” and “squeezes” objects that reside in that space, a behavior analogous to the tidal effects exerted by the Moon on Earth. If an object is small compared to the wavelength of GWs, then waves exert tidal forces with a quadrupolar pattern. The dimensionless strength h of the wave can be estimated using the quadrupole approximation, e.g., $h \simeq (G/c^4)\ddot{Q}/r$, where \ddot{Q} is the second derivative of the source’s quadrupole moment and r is the distance to the source. Gravitational waves carry away from their sources not only energy but also angular and linear momenta. The weakness of the gravitational interactions explains the difficulty of detecting GWs, which propagate practically without being scattered or absorbed by matter. Thanks to the transparency of media to GWs, the deep interior of neutron stars or the neighborhood of merging black holes can be probed as well as physical processes in the very early universe. An indirect proof of the existence of

GWs was provided by measurements of the secular changes in the orbital parameters of the binary pulsar PSR 1913+16, which agrees with predictions of the GRT to within 1% accuracy (Hulse & Taylor 1975; Taylor & Weissberg 1989).

The search for a direct detection of GWs began with the pioneering work by Weber (1960), who used a resonant mass detector. In the early seventies, the idea emerged that laser interferometers might have a better chance of detecting GWs (Weiss 1971; Moss et al. 1971). Presently, the first generation of ground-based laser interferometers, such as TAMA300 (Kuroda et al. 1997), LIGO (Abramovici et al. 1992) and VIRGO (Bradaschia et al. 1990), are operational and gravitational wave astronomy is becoming a reality, in spite of the fact that no direct detection has been achieved up to date. A fundamental upgrade of the present technology is required to reach the ultimate sensitivity that will permit the detection of signals from a representative volume of the universe. This includes new materials, high-powered lasers, diffractive optics and cryo-techniques. More ambitious projects are presently in development or under discussion, including the Laser Interferometer Space Antenna (LISA), a collaboration between the European Space Agency (ESA) and the National Aeronautics and Space Administration (NASA), and the next generation of ground-based interferometers like the advanced LIGO or cryogenic laser interferometers, such as the Japanese LCGT or the European Einstein gravitational antenna. Besides laser interferometers, new concepts of broadband resonant mass detectors have been put forward (Cerdonio et al. 2001; Bonaldi et al. 2003). A massive sphere is suspended inside a second hollow one and short, high-finesse Fabry-Perot optical cavities read out the differential sphere displacements as their quadrupole modes are excited. Theoretical estimates indicate that a molybdenum detector with an overall size of 2 m, would reach spectral strain sensitivities of $\sim 2 \times 10^{-23} \text{ Hz}^{-1/2}$ in the frequency range 1–3 kHz.

The detected gravitational signal depends on the relative orientation between the detector and the source, being expressed as

$$h(t) = h_+(t)F_+(\theta, \phi, \psi) + h_\times(t)F_\times(\theta, \phi, \psi), \quad (1)$$

where F_+ and F_\times are the beam factors, which are functions of the source coordinates, the zenith distance θ and the azimuth ϕ , as well as of the wave polarization plane orientation ψ (see, for instance, Jaranowski et al. 1998, for details). The observation of a GW signal in a noisy detector entails the measurement of the signal properties in the presence of a particular instance of the detector noise. The best signal-to-noise (S/N) ratio that can be achieved implies the use of techniques such as “matched filtering,” which depends on the nature of the signal. The basic idea of this procedure is to correlate the observed signal \mathbf{s} to theoretical *templates* h_T , which represent the expected source waveform. If the “match,” namely the correlation between the observed signal and a given template, is much higher than the correlation between the observed signal and the detector noise, then a gravitational wave detection has occurred.

Burst sources associated to cosmic catastrophes, like a gravitational collapse, emit gravitational radiation at some characteristic frequency but in a very short time. Quasi-periodic sources like close binary systems, emit gravitational radiation over a longer time interval but generally produce weaker signals. However, if the waveform is known or can be modeled, the source can be followed during many cycles, considerably improving the S/N ratio.

In this paper, the properties of potential GW sources that have been discussed in the literature in the past years are reviewed, as well as the expected detectability by the major interferometers presently in operation around the world or by those still under consideration, either in space or on the ground. Gravitational wave sources are generally classified in two categories (“burst” and “quasi-periodic”): “burst” and “quasi-periodic” sources as mentioned above or alternatively, equivalent categories ($10^{-4} \sim 10^{-1} \text{ Hz}$) and “high” ($1 \sim 10^4 \text{ Hz}$) frequency sources. The former correspond to frequencies in the range of space experiments like LISA, while the latter correspond to frequencies covered by most ground based laser interferometers. Here, GW sources will be studied according to their association with known astrophysical objects. In Section 2, the core collapse of massive stars

and the consequent formation of either a neutron star (NS) or a black hole (BH) are discussed; in Section 3, the different GW emission mechanisms associated with fast rotating NSs are analyzed; in Section 4, sources associated with binary systems consisting of two compact objects are examined and, finally, in Section 5, the main conclusions are given.

2 CORE COLLAPSE

2.1 Formation of Neutron Stars

When the core of a massive star has exhausted its supply of nuclear fuel, it collapses to form, according to its initial mass, either a neutron star or a black hole. Besides the initial mass, the outcome of the core collapse depends on the angular momentum and metallicity of the progenitor. Three distinct phases can be identified:

- (1) *The infall* of the iron core having a mass close to the Chandrasekhar limit ($\simeq 1.4 M_{\odot}$). The infall of the inner layers stops when the very central core reaches the nuclear matter density but in fast rotating cores, centrifugal forces may stop the collapse before the nuclear matter density is reached.
- (2) The sudden “stiffness” of the equation of state produces a *bounce* of the infalling matter and a reverse shock develops at the edge of the inner core, defined by the shell where the infall velocity is equal to the local sound velocity.
- (3) Finally, the *oscillatory* phase, in which the core oscillates with a superposition of various radial and surface modes (see, for instance, Zwerger & Muller 1997). This quasi-periodic phase could last for hundreds of oscillation periods before effectively being damped.

Theoretical stellar evolutionary tracks at advanced phases are still uncertain but NSs are expected to be formed in the collapse of stars more massive than $9 M_{\odot}$. The upper limit is more uncertain, but is expected to be situated around $40\text{--}50 M_{\odot}$ or, in other words, stars more massive than these values will probably collapse into a BH. It is interesting to notice that the binary X-ray pulsar GX301-2 has a B1 supergiant (Wray 977) as a companion. From an estimate of the present mass of Wray 977, Kaper et al. (1995) were able to obtain a lower limit of $50 M_{\odot}$ for BH formation. This conclusion is probably not a robust one, since in mass exchange processes in the early evolutionary phases of the system, it is difficult to estimate the original masses. However, the discovery of the X-ray pulsar (CXO J1647-45) in the young galactic cluster Westerlund-1 (Muno et al. 2005) defines a secure estimate of the mass of the NS progenitor of about $40 M_{\odot}$, based on the cluster age. Since there are no evidences for a companion with $M > 1 M_{\odot}$, this limit is not affected, as in the previous case, by mass exchange processes, which implies that stellar BHs probably originated from progenitors more massive than $40 M_{\odot}$.

The formation of a NS releases about 10^{53} erg carried out essentially by MeV-neutrinos, which transfer momentum to the star’s mantle, triggering the explosive ejection of these outer layers and giving rise to a supernova. An eventual detection of both neutrinos and GW bursts would be an unambiguous signature of the gravitational collapse.

Although there is little doubt that a core-collapse produces GWs, the characteristics of the signal are difficult to estimate. The rotation rate of the collapsing star directly affects the emission rate and the choice of the pre-collapse angular velocity can make a large difference in the strength of the GW signal. Muller & Janka (1997) performed 3+1 dimensional simulations of the gravitational collapse and estimated an amplitude $h \simeq 4 \times 10^{-23} (10 \text{ kpc } r^{-1})$, which is a consequence of a relatively small flattening. In fact, recent studies (Hirschi et al. 2004; Heger et al. 2005) indicate that stellar iron cores rotate more slowly than previously assumed and that the asphericity is not enough to produce a sizeable mass-quadrupole moment. These results indicate that only events occurring in our Galaxy are likely to produce a gravitational signal able to be detected by the present generation of laser

interferometers. It is worth mentioning that even if a non-rotating core collapses, a convective and unstable neutron star can be formed (Burrows & Hayes 1996; Muller et al. 2004). In this situation, the fluid at nuclear matter density “boils” during the very first seconds, dredging up high temperature material ($T \sim 10^{12}$ K), which cools by neutrino emission before being swept back downward and reheated. Such a boiling generates ~ 100 cycles of GWs with a frequency ~ 100 Hz and amplitude large enough to be detected either by VIRGO or LIGO throughout our Galaxy and its satellites.

Long-term 2D axisymmetric simulations in the post-bounce phase of a core-collapse have been performed by Kotake et al. (2007), aiming to study asphericities induced by the growth of instabilities in the accretion shock region. These instabilities produce an anisotropic neutrino emission, which increases the amplitude of GWs up to two orders of magnitude larger than those originating from the aforementioned convective motion and could be detected by advanced interferometers for a typical source distance of ~ 10 kpc.

More recently, axisymmetric 2D Newtonian radiation-hydrodynamic simulations (Burrows et al. 2007) indicate that the dominant emission process of GWs during the core-collapse may be the oscillations of a protoneutron star. These oscillations are predominantly g -modes excited hundreds of milliseconds after the bounce and lasting typically for several hundred milliseconds. Supernova models with progenitors having 11, 15 and 25 M_{\odot} respectively have been modeled by Ott et al. (2006). Their results suggest that the total energy released in the form of GWs depends on the progenitor mass and can attain values up to $8.2 \times 10^{-5} M_{\odot} c^2$ with characteristic frequencies in the range 650–940 Hz. According to these calculations, the gravitational signal of collapsing massive stars can be detected up to distances on the order 1 Mpc or up to M31, the Andromeda galaxy.

Another mechanism able to produce GWs refers to the “ringing” of a NS excited by the fall-back accretion of material not expelled during the supernova explosion. Rotation and convective motions break the spherical symmetry of the accretion flow and different oscillation modes will be excited in the process. The 2D nonlinear hydrodynamical simulations of NS ringing have been performed by Nagar et al. (2004), who have shown that the gravitational wave signal comprises the $l = 2$ mode and high frequency interference fringes, related to the motion of the infalling matter. The total emitted GW energy is comparable to the amount released immediately after the core bounce.

It is worth mentioning that other stellar collapse scenarios are possible as, for instance, that of a white dwarf whose mass is pushed just beyond the Chandrasekhar limit via accretion (accretion induced collapse, or AIC, see Liu & Lindblom 2001). In this case, as the star collapses, its temperature increases adiabatically until reaching a limit imposed by the neutrino cooling. If neutrino losses are not sufficient to control the adiabatic heating, the temperature will increase up to values able to ignite nuclear reactions and the entire white dwarf explodes as a type Ia supernova. However, if neutrino losses are able to prevent the nuclear burning, electrons are captured onto protons during the contraction and a neutron star will ultimately be formed. This is an evolution very similar to the core-collapse of massive stars. Some fraction of collapsing white dwarfs will produce supernovae while others will form NSs. Their evolutionary path sensitively depends upon the initial white dwarf mass, its chemical composition and the rate at which it accretes mass. An upper limit on the rate of AICs in the Galaxy of about 10^{-5} yr^{-1} was estimated by Fryer et al. (1999), implying that these events have quite a small detection probability.

2.2 Formation of Black Holes

Black holes are expected to exist in our universe within a large mass interval. Stellar black holes may directly be formed in the core collapse of massive stars, by accretion of NSs, and by the merging of two NSs at the end point of their inspiral in a binary system, whereas very massive BHs, probably present in all galactic nuclei, are mainly formed by successive coalescences after merger events of their respective host halos and by accretion of the gas present in the central regions of galaxies.

Past 2D-hydrodynamic simulations of core collapses by Fryer (1999) suggest that for a large range of progenitor masses, the partial fall back of the envelope drives the compact core to collapse into a BH. The newly formed BH is likely to be quite “distorted” from the quiescent Kerr form and remains so as material falls back onto it. The “distortion” drives the BH to radiate GWs as it settles down to a Kerr configuration. The waveform of the initial burst depends on the details of the collapse, but the late time behavior (the “ring-down” phase) has a well established damped oscillatory form, which is essentially a function of the BH mass M_{bh} and angular momentum J (Echeverria 1989). If mass accretion significantly increases the BH mass during the ring-down, the decay rate and mode-frequencies are modulated by the matter inflow and the frequency evolution pattern reveals features which depend not only on the accretion rate but also on the total accreted mass (Papadopoulos & Font 2001). The emitted waves are a superposition of spheroidal modes, with the quadrupole mode ($l = 2$) being dominate, while the dominant m -mode depends upon the matter flow. The $m = \pm 2$ modes are bar-like co-rotating (+) or counter-rotating (−) with the BH spin. For the main quasi-normal mode ($l = m = 2$), the frequency and the quality factor $Q = \pi\nu_{\text{gw}}\tau_{\text{gw}}$ are respectively given by the approximate expressions (Echeverria 1989)

$$\nu_{\text{gw}} \simeq 12 \left(\frac{M_{\odot}}{M_{\text{bh}}} \right) F(a) \text{ kHz}, \quad (2)$$

and

$$Q = K(a) \simeq 2(1 - a)^{-0.45}, \quad (3)$$

where $a = Jc/GM^2$ and $F(a)$ is given by

$$F(a) \simeq \left[\frac{100}{37} - \frac{63}{37}(1 - a)^{0.3} \right]. \quad (4)$$

The amplitude of the ring-down wave depends on the way and extent to which the BH is “distorted”. Here, we assume that the total emitted energy corresponds to a fraction ε of the BH mass, e.g., $E = \varepsilon M_{\text{bh}} c^2$. In this case, assuming a damped sinusoidal waveform, the amplitude of the signal is

$$h_0 = 5.57 \times 10^{-21} \left(\frac{10 \text{ Mpc}}{D} \right) \left(\frac{M_{\text{bh}}}{M_{\odot}} \right) \sqrt{\frac{\varepsilon}{K(a)F(a)}}, \quad (5)$$

where D is the distance-luminosity in Mpc.

Using a “matched-filtering” technique, the expected S/N ratio is

$$\left(\frac{S}{N} \right)^2 = \frac{4}{5} h_0^2 \left[\frac{\tau_{\text{gw}}}{S_n(\nu_{\text{gw}})} \right] \frac{Q^2}{1 + 4Q^2}, \quad (6)$$

where $Q = \pi\nu_{\text{gw}}\tau_{\text{gw}}$ is the quality factor of the oscillation, $S_n(\nu)$ is the noise power spectrum of the detector; the angle averaged beam factors of the detector were already included. Equations (5) and (6) permit an estimate of the maximum distance that a given event can be detected once the S/N ratio, the radiation efficiency ε , the mass and the angular momentum of the BH are fixed.

In order to perform some numerical estimates, a typical stellar BH of mass $9 M_{\odot}$ will be considered and a signal-to-noise ratio S/N=5 will be required. Head-on collisions between a BH and an NS have been considered in a fully relativistic approach by Loffler et al. (2006). They have estimated a GW efficiency for the ring-down emission of about 7.8×10^{-4} , which will be adopted here. Table 1 compares the maximum distances that are expected to be probed by advanced interferometers like EGO or Advanced LIGO for two values of the spin parameter a .

These estimates indicate that even advanced laser beam interferometers are not able to probe the ringdown emission beyond the Local Universe, implying that the expected event rate is quite low. The reason is that the ring-down has a very low quality factor ($Q \sim 2 - 4$) and, at frequencies around 1.4–2.0 kHz, laser interferometers are dominated by photo-electron shot noise. That range is less sensible than at frequencies around 150–250 Hz, the domain in which the mirror thermal noise prevails and where the sensitivity is maximum.

Table 1 Maximum Expected Distances at which a “Ringdown” Signal Can Be Detected with an S/N=5

a	ν_{gw} (kHz)	τ_{gw} (ms)	D_{EGO} (Mpc)	D_{AdL} (Mpc)
0.02	1.35	0.48	6.9	0.94
0.50	1.76	0.49	4.1	0.54

3 ROTATING NEUTRON STARS

3.1 Tri-Axial Stars

Historically, neutron stars, which are known to be quite abundant in the Galaxy, were ranked among conspicuous emitters of GWs. Rotating NSs may have a time-varying quadrupole moment and hence radiate GWs, by either having a triaxial shape or a misalignment between the symmetry and spin axes, which produces a wobble in the stellar motion. Moreover, fast and hot rotating proto-neutron stars may develop different instabilities, such as the so-called Chandrasekhar-Friedman-Schultz (CFS) instability (Andersson & Kokkotas 2001, and references therein), which is responsible for the excitation of density waves traveling around the star in the sense opposite to its rotation, or undergo a transition from axi-symmetric to triaxial shapes through the dynamical “bar-mode” instability (Lai & Shapiro 1995). All these mechanisms are potentially able to emit a considerable amount of energy in the form of GWs. In the case of a rotating triaxial NS, the gravitational strain amplitude of both polarization modes is given by

$$h_{+}(t) = 2A(1 + \cos^2 \beta) \cos(2\Omega t), \quad (7)$$

and

$$h_{\times}(t) = 4A \cos \beta \sin(2\Omega t), \quad (8)$$

where β is the angle between the spin axis and the wave propagation vector, assumed to coincide with the line of sight, Ω is the angular rotation velocity and the amplitude A is defined by

$$A = \frac{G}{Dc^4} \epsilon I_{zz} \Omega^2, \quad (9)$$

where D is the NS distance, I_{zz} is the moment of inertia and the ellipticity ϵ is defined by

$$\epsilon = \frac{I_{xx} - I_{yy}}{I_{zz}}. \quad (10)$$

Notice that the frequency of the GWs is twice the rotation frequency of the NS.

Detection of both polarization modes of a radio pulsar immediately leads to the value of the spin projection angle β and to an estimate of the ellipticity, if the distance is known by measuring the dispersion of radio signals through the interstellar plasma. Upper limits on the ellipticity ϵ have been obtained by assuming that the observed spin-down of pulsars is essentially due to the emission of GWs. In this case, for “canonical” pulsars, one obtains $\epsilon \leq 10^{-3}$ whereas “recycled” millisecond pulsars seem to have equatorial deformations less than 10^{-8} . Monte Carlo simulations of the galactic pulsar population by Regimbau & de Freitas Pacheco (2000, 2003) indicate that for integration times on the order of 10^7 s, significant detections by VIRGO are only possible if the mean pulsar ellipticity is on the order of 10^{-6} . Recently, the LIGO team (Abbott et al. 2007) reported upper limits for the amplitude of gravitational waves from 78 isolated radio pulsars, which can be translated into limits for ellipticities. For instance, J1024–07 and J2124–33 respectively have ellipticities less than $\epsilon < 1.0 \times 10^{-6}$ and $\epsilon < 7.0 \times 10^{-7}$, consistent with the results derived from the aforementioned simulations.

Most of these upper limits are higher than values derived under the assumption that the observed rotation breaking is essentially due to the emission of gravitational waves, with the exception of the Crab pulsar. In this case, the derived upper limit permits researchers to impose strong constraints on the initial rotation period of the pulsar as well as on its magnetic field. It is well known that in the case of the Crab, the magnetic dipole breaking age (~ 1330 yr) is higher than the “true” age (~ 950 yr). Such a discrepancy led Ostriker & Gunn (1969) to suggest that the gravitational radiation contributed as an extra breaking mechanism almost forty years ago. From the equations of motion, the ratio between the breaking age $t_* = 2P/\dot{P}$ and the “true” age t_a can be written as

$$\left(\frac{t_a}{t_*}\right) = \left(\frac{1 + \eta x_a^2}{\eta x_a^2}\right) \left[x_a^2 - 1 - \frac{1}{\eta} \ln \left(\frac{1 + \eta x_a^2}{1 + \eta} \right) \right]. \quad (11)$$

In this equation, the left side is known from observations ($t_a/t_* = 0.7157$), $x_a = P_a/P_0$ is the ratio between the present P_a (observed) and the initial P_0 rotation periods and η is the ratio between the breaking timescales (gravitational and magnetic dipole), explicitly given by

$$\eta = \frac{5}{768\pi} \frac{(B \sin \alpha)^2 R^6 P_0^2}{GI_{zz}^2 \epsilon^2}. \quad (12)$$

The numerical solution of Equation (11) gives pairs (x_a, η) which can be converted into pairs involving the ellipticity and the projection of the magnetic field along the spin axis ($B \sin \alpha$). Then, using the observed upper limit for the Crab ellipticity derived from run S5, i.e., $\epsilon < 2.6 \times 10^{-4}$ and values for the radius and moment of inertia for a “canonical” neutron star, the following parameters are derived: initial rotation period $P_0 = 24.9 \pm 0.6$ ms and $B \sin \alpha = (8 \pm 1) \times 10^{12}$ G.

Different scenarios leading to a distorted star have been discussed in the literature, as anisotropic stresses from strong magnetic fields and tilting of the symmetry axis during the initial cooling phase when the crust of the proto-neutron star solidifies. Bildsten (1998) pointed out that a NS in a state of accretion may develop non-axisymmetric temperature variations on the surface, which produce horizontal density patterns able to create a large mass quadrupole moment, if the elastic response of the crust is neglected. More detailed calculations (Ushomirsky et al. 2000) indicate that the inclusion of the crustal elasticity decreases the expected mass quadrupole by a factor of 20–50, considerably reducing the predicted GW emission. Elastic deformations of compact objects with “exotic” equations of state have been considered by Owen (2005). He showed that solid strange stars could sustain ellipticities as high as a few times 10^{-4} , considerably higher than estimated values for conventional NSs (Thorne 1980). More recently, Horowitz & Kadau (2009) have revisited the breaking strain of the crust of neutron stars, reaching the conclusion that ellipticities up to 4×10^{-6} can be supported by canonical neutron stars, consistent with the early analyses by Regimbau & de Freitas Pacheco (2000, 2003).

The distortion induced by magnetic fields becomes significant in highly magnetized NSs, overwhelming the flattening due to a fast rotation. The existence of NSs with magnetic fields in excess of 10^{14} G (dubbed magnetars) was firstly suggested by Thompson & Duncan (1993). They have shown that in fast newborn NSs, the dynamo mechanism could generate magnetic field strengths up to 10^{16} G. The existence of magnetars is supported by the observation of “soft gamma repeaters” (SGRs) and anomalous X-ray pulsars (AXPs), whose rotation periods and deceleration rates, if interpreted in terms of the canonical magnetic dipole model, suggest that these objects are associated with young highly magnetized NSs (Kouveliotou et al. 1998, 1999; de Freitas Pacheco 1998; Heyl & Kulkarny 1998; Mereghetti 1999). On one hand, magnetars may be considered as objects having an origin and evolutionary path different from canonical radio pulsars but, on the other hand, population synthesis simulations by Regimbau & de Freitas Pacheco (2001, 2006) suggest that NSs are born with a large variety of rotational periods and magnetic fields and that magnetars are objects simply born on the high tail side of the magnetic field distribution. Figure 1 shows the observed magnetic

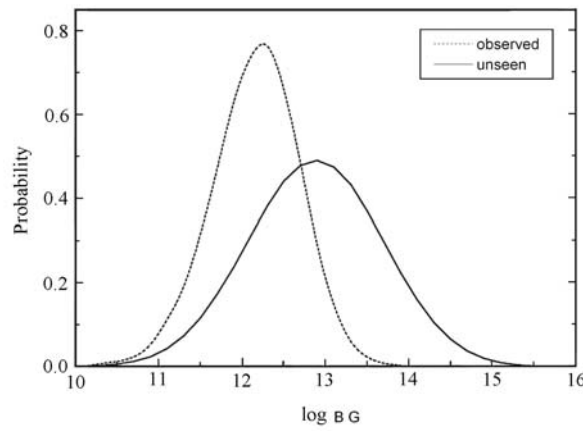


Fig. 1 Magnetic field distribution of observed pulsars (*dashed curve*) and that for the unseen (real) population (*solid curve*). Adapted from Regimbau & de Freitas Pacheco (2006).

field distribution as well as that for the “unseen” population, hidden by a different observational bias. The mean field of the observed population is about 1.6×10^{12} G and the distribution has an apparent cutoff around 10^{14} G. The hidden population has an average magnetic field one order of magnitude higher and the estimated fraction of magnetars, defined as objects with fields above 10^{14} G, is about 8% of the total pulsar population, which amounts to $\sim 250\,000$ objects. This number should not be identified with the total number of NSs in the Galaxy, which is evidently several orders of magnitude higher.

The deformation of magnetized Newtonian stars was already discussed in the early fifties by Chandrasekhar & Fermi (1953) and Ferraro (1954). The GW emission from magnetic distorted stars was considered by Gal’tsov & Tsvetkov (1984), Bonazzola & Gourgoulhon (1996), Konno et al. (1999, 2000), and Palomba (2001), among others. The deformation of a slowly rotating magnetized star can be expressed as the sum of the contribution of three main terms: the first and the most important corresponds to the Lorentz force, induced by current flows in the highly conductive NS interior; the second term represents variations of the gravitational potential, a consequence of the distortion itself; and, finally, the third is a purely relativistic term arising from the definition of the circumferential radius $R = L/2\pi$, where L is the length of the equator as measured by a non-rotating observer. In general, the ellipticity induced by magnetic field effects can be expressed by the dimensionless ratio (Konno et al. 2000)

$$\epsilon_B = g \frac{B^2 R^4}{GM^2} \sin^2 \alpha = 1.9 \times 10^{-8} g B_{14}^2 R_{10}^4 M_{1.4}^{-2} \sin^2 \alpha, \quad (13)$$

where B , R and M are respectively the magnetic field at the surface, the radius and the mass of the NS, α is the angle between the spin and the magnetic dipole axes, while g is a dimensionless parameter depending both on the equation of state and on the magnetic field geometry. In the case of an incompressible fluid star with a dipole field, the deformation parameter is $g = 12.5$. Relativistic models based on a polytropic equation of state and a dipole field geometry give similar values (Konno et al. 2000). NS models built with the equation of state UV₁₄+TNI (Wiringa et al. 1988) and with non-superconducting NS matter lead to deformation parameters g on the order of the unity for currents concentrated in the crust and a few times higher if currents are concentrated in the core (Bonazzola & Gourgoulhon 1996). These values correspond to ellipticities of about $(2 - 20) \times 10^{-8}$ for fields typically on the order of 10^{14} G, below the limits estimated by Regimbau

& de Freitas Pacheco (2000, 2003), to produce a detectable signal by the present generation of interferometric detectors. If NSs have a superconducting interior of type I, the magnetic field permeates only the very outer layers of the star and distortion parameters as high as $g \simeq 520$ can be obtained (Bonazzola & Gourgoulhon 1996), corresponding to ellipticities on the order of 10^{-5} for magnetic fields of $\sim 10^{14}$ G. However, magnetars have a rather strong magnetic dipole braking and they are only “visible” by the detector on the low frequency side for a very short time interval, considerably reducing the detection probability.

3.2 Bar Modes

Fast rotating NSs may develop non-axisymmetric instabilities if the ratio between the rotational and gravitational energies, $\beta = T/|W|$, is higher than a certain critical value. These instabilities correspond to global non-radial toroidal modes with eigenfunctions $\propto e^{\pm im\phi}$, where $m = 2$ is the so-called bar-mode, the fastest growing mode when rotation is very rapid. They are called bar-modes since they give an elongated shape to the star. NSs may become dynamically unstable against bar modes when $\beta_d > 0.27$ (the hydrodynamic time scale determines the instability evolution) or secularly unstable under dissipative processes such as viscosity or gravitational radiation when $\beta_s \geq 0.14$ (the shorter dissipation time scale determines the instability evolution). These limits have been rigorously derived for homogeneous and uniformly rotating Newtonian stars, but further relativistic numerical studies using polytropic equations of state and assuming ad-hoc rotation profiles lead to the conclusion that the onset of the dynamical instability occurs approximately at the same limit (Houser et al. 1994; Shibata et al. 2000), but relativistic effects tend to strengthen the secular instability. In fact, Morsink et al. (1999) found that, for a wide range of “realistic” equations of state, the critical value of β_s can be fitted by the relation

$$\beta_s \simeq 0.115 - 0.048 \frac{M}{M_{\max}}, \quad (14)$$

where M_{\max} is the possible maximum mass of a stable non-rotating star issued from a given equation of state. On the other hand, Centrella et al. (2001) found low- β instabilities, which seem to be associated with the presence of corotation points and that may be excited if centrifugal forces produce a density peak off the rotation center. Moreover, rotating stars with differential rotation may also become dynamically unstable even if $\beta \sim 0.01$ (Shibata et al. 2002, 2003).

The bar-mode instability can be excited in a hot proto-NS a few milliseconds after the core bounce or a few tenths of seconds later, when the star has cooled by neutrino emission and contracted, with β becoming larger than the critical value. The instability develops in two steps (Houser et al. 1994): i) after shedding mass in the form of two spiral arms which merge in the equatorial plane and inducing angular momentum losses, the system evolves toward an axisymmetric state (MacLaurin spheroid) which is dynamically stable but still secularly unstable; ii) the star becomes a Dedekind or a Jacobi ellipsoid depending on whether the instability is driven by gravitational radiation or viscosity. As the star evolves toward a Dedekind ellipsoid, hydrodynamic waves propagate counterclockwise through the external layers.

Most of the numerical studies suggest that after the dynamical instability phase (if the system was initially set beyond the limit $\beta \simeq 0.27$), it recovers almost an axisymmetric shape, but with β still above the secular instability threshold. In this case, the system may evolve away from the axisymmetric configuration in a time scale determined by the gravitational radiation reaction, which is of the order of *a few seconds* for β in the range 0.20–0.25, as simulations suggest. This evolutionary path is possible if the gravitational radiation overcomes viscosity. Then, during the evolution, the fluid circulation is conserved (but not angular momentum) and the system evolves toward a Dedekind ellipsoid, whose configuration is a fixed triaxial figure with an internal fluid circulation of constant vorticity. In the opposite situation, when the viscosity drives the instability, angular momentum is

conserved but not the fluid circulation, and the system evolves toward a Jacobi ellipsoid. The transition to a Dedekind configuration is manifested in the form of strong hydrodynamic waves in the outer layers and mantle, propagating in the opposite direction of the star's rotation. The frequency of GWs is maximum at the beginning of the transition ($\nu_{\max} \sim 800$ Hz) and then it decreases monotonically. Since GWs carry away angular momentum, the final configuration is a non-rotating triaxial ellipsoid, which no longer emits GWs. Thus, the wave amplitude first increases, reaches a maximum when $\nu \sim 500$ Hz, and then decreases to zero. Lai & Shapiro (1995) estimated that the total GW energy radiated during the transition could be as high as $4 \times 10^{-3} \text{ Mc}^2$ in a typical time scale of ~ 120 s. Estimates of the characteristic gravitational strain amplitude for the dynamical instability phase performed by different authors (Houser et al. 1994; Houser & Centrella 1996; Brown 2000; Shibata et al. 2000) seem to be in rough agreement, e.g., they predict a characteristic amplitude $h_c \simeq 3 \times 10^{-22}$ at a distance of 20 Mpc.

More recently, the above picture, based on the behavior of an incompressible fluid star, has been questioned by hydrodynamic simulations using a post-Newtonian approach, a polytropic equation of state with index $N = 1$ and non-uniform rotation (Shibata & Karino 2004). In fact, for $N > 0.8$, the Dedekind configuration may not exist because: a) the uniformly rotating Jacobi ellipsoid does not exist for $N > 0.808$ (James 1964) or b) the Dedekind theorem for incompressible fluids says that the absence of the Jacobi configuration implies the absence of the Dedekind ellipsoid. In this case, it is possible that a secularly unstable star relaxes to a nearly axisymmetric stable rotating star, after sufficient angular momentum losses by gravitational waves, as the simulations by Shibata & Karino (2004) suggest. According to these authors, the characteristic frequency of gravitational waves emitted by a secularly unstable star is

$$\nu_{\text{gw}} \simeq 460 \left(\frac{\sigma}{0.6 \rho_c^{1/2}} \right) \left(\frac{R_e}{20 \text{ km}} \right)^{-3/2} \left(\frac{M}{1.4 M_\odot} \right)^{1/2} \text{ Hz}, \quad (15)$$

where σ is the angular velocity of the non-axisymmetric perturbation in units of $\rho_c^{1/2}$, the square root of the initial central density of the star, and R_e is the equatorial radius. The effective amplitude of GWs is $h_{\text{eff}} = N_c^{1/2} h$, with N_c being the number of cycles of the GW train and h is the characteristic amplitude, e.g.

$$h_{\text{eff}} \simeq 5.2 \times 10^{-22} \left(\frac{\zeta}{0.2} \right)^{1/2} \left(\frac{R_e}{20 \text{ km}} \right) \left(\frac{M}{1.4 M_\odot} \right)^{1/2} \left(\frac{\nu_{\text{gw}}}{460 \text{ Hz}} \right)^{1/2} \left(\frac{100 \text{ Mpc}}{D} \right), \quad (16)$$

where $\zeta \sim 0.2$ is a dimensionless parameter. Under these conditions, the expected signal-to-noise ratio is

$$\frac{S}{N} \simeq \frac{2h_{\text{eff}}}{\sqrt{\nu S_n(\nu)}}. \quad (17)$$

Fixing $S/N=7$, the maximum luminosity-distances probed by VIRGO and LIGO are respectively 15 Mpc and 12 Mpc. The expected event rate is approximately given by the product of the type II supernova rate inside a volume of radius 12–15 Mpc and the fraction ζ_{bar} of NSs born with initial periods within the instability window. The former factor, using the results by Cappellaro et al. (1999), corresponds to about 4.0 supernova yr^{-1} , while the latter can be estimated from the relation

$$\zeta_{\text{bar}} = \int_{P_1}^{P_2} g(P) dP, \quad (18)$$

where $g(P) \propto \exp[-(P - \bar{P})^2/2\sigma^2]$ is the probability distribution of initial rotation periods (see Regimbau & de Freitas Pacheco 2000), whose updated parameters are $\bar{P} = 240 \pm 20$ ms and $\sigma = 80 \pm 20$ ms. For a canonical NS, the instability interval ($0.1375 \leq \beta \leq 0.2738$) corresponds to a

very narrow interval of rotation periods, e.g., (0.82–1.14) ms. Therefore, $\zeta_{\text{bar}} = 3.6 \times 10^{-6}$ and the expected event rate for LIGO and VIRGO is rather small, e.g., in the range of 14 events per Myr.

For the planned advanced detectors, the maximum probed luminosity-distance ($S/N=7$) corresponds to 144 Mpc for ad-LIGO and 742 Mpc ($z \simeq 0.152$) for EGO. The expected detection rate for ad-LIGO is still rather small (one every 230 yr) and, in the case of EGO, evolutionary effects on the cosmic star formation rate must be taken into account. Thus, the expected event rate R_{bar} is given by the equation

$$R_{\text{bar}} = 4\pi\lambda_{\text{ns}}\zeta_{\text{bar}}\frac{c}{H_0} \int_0^{z_{\text{max}}} \frac{R(z')}{(1+z')} \frac{r(z')^2}{E(z')} dz', \quad (19)$$

where $\lambda_{\text{ns}} = 5.7 \times 10^{-3} M_{\odot}^{-1}$ is the fraction by mass of NS progenitors (stars in the mass range 9–40 M_{\odot}), weighted by a Salpeter's initial mass function. $R(z)$ is the cosmic star formation rate (in $M_{\odot} \text{ Mpc}^{-3} \text{ yr}^{-1}$ and, in our calculations, the parameterization given by Hopkins & Beacom 2006 was used), the term $(1+z)$ in the denominator takes into account time dilation, $r(z)$ is the comoving distance and $E(z) = \sqrt{\Omega_{\Lambda} + \Omega_m(1+z)^3}$ corresponds to a flat cosmology ($\Omega_{\Lambda} + \Omega_m = 1$). Performing the integral, one obtains about one event every two years, if the planned sensitivity will in fact be achieved.

3.3 r-Modes

The r-mode (r for rotation) is a member of a class of gravitational radiation driven instabilities (including the secular bar-mode instability) excited by the so-called CFS (Chandrasekhar-Friedman-Schultz) mechanism. These large scale toroidal fluid oscillations are similar to the well known geophysical Rossby waves whose restoring force is the Coriolis force (Stergioulas 2003, and references therein). The mechanism for the gravitational wave instability can be understood in the following way. The eigen-frequencies of the mode are $\pm\omega$, corresponding to $\pm m$ and corresponding to the forwards and backwards propagating modes. These two modes are affected differently by the rotation of the star. The backwards mode will be dragged forwards by the stellar rotation, and if the star spins sufficiently fast, the perturbation will move forwards with respect to the inertial frame while still moving backwards in the rotating frame. The GWs from such a mode carry positive angular momentum away from the star, but since the perturbed fluid rotates slower than it would in the absence of the perturbation, the angular momentum of the retrograde mode is negative. Thus, the emission of GWs makes the angular momentum of the mode increasingly negative, leading to an instability. Once the disturbances radiate away the star's angular momentum, the system can find a state of lower energy and angular momentum. The fact that the emission of GWs causes a growth in the mode energy in the rotating frame E_r , despite that the decrease in the inertial frame energy E_i can be understood from the relation expressing the energy in both frames, e.g.,

$$E_r = E_i - J\Omega. \quad (20)$$

This relation says that E_r may increase even if both E_i and J decrease. The r-mode velocity field measured by a co-rotating observer is approximately given by

$$\delta\mathbf{v}(r, t) \simeq \alpha\Omega R \left(\frac{r}{R}\right)^m \mathbf{Y}_{mm}^B e^{i\omega_r t}, \quad (21)$$

where α is the dimensionless amplitude of the perturbation and \mathbf{Y}_{ml}^B is the magnetic multipole as defined by Thorne (1980). The r-mode ($l = m$) frequency ω_r is related to the star's rotation velocity by

$$\omega_r \simeq \frac{2m\Omega}{l(l+1)} \left[1 - 0.573 \frac{\Omega^2}{\pi\rho} \right]. \quad (22)$$

In the first seconds after the formation of the NS, the temperature is very high ($T \sim 10^{11}$ K) and the bulk viscosity is expected to suppress the CFS instability, whereas the shear viscosity plays a stabilizing role for temperatures $T \leq 10^9$ K. Thus, there is a well defined window in which a fast newly-born NS is unstable. As the star cools by neutrino emission and decelerates by GW emission, it stabilizes around periods of 15–25 ms. According to this scenario, no newly-born pulsar faster than this limit should be observed. However, these estimates depend not only on damping effects due to different physical mechanisms, with most of them still badly understood, but also on the role played by the crust and magnetic field.

In the plane Ω – T , the instability limit region can roughly be estimated by imposing that the energy rate balance of the mode is zero, e.g.,

$$\frac{1}{\tau} = \frac{1}{\tau_{\text{gr}}} + \frac{1}{\tau_{\text{b}}} + \frac{1}{\tau_{\text{s}}} = 0, \quad (23)$$

where τ_{gr} , τ_{b} and τ_{s} are respectively the gravitational radiation, and the bulk and shear viscosity damping time scales. For the $m = 2$ mode, these time scales are approximately given by Andersson & Kokkotas (2001)

$$\tau_{\text{gr}} = -22 \left(\frac{1.4 M_{\odot}}{M} \right) \left(\frac{10 \text{ km}}{R} \right)^4 \left(\frac{P}{1 \text{ ms}} \right)^6 \text{ s}, \quad (24)$$

$$\tau_{\text{b}} \simeq 2.7 \times 10^{11} \left(\frac{M}{1.4 M_{\odot}} \right) \left(\frac{10 \text{ km}}{R} \right) \left(\frac{P}{1 \text{ ms}} \right)^2 \left(\frac{10^9 \text{ K}}{T} \right)^6 \text{ s}, \quad (25)$$

and

$$\tau_{\text{s}} \simeq 1.2 \times 10^8 \left(\frac{1.4 M_{\odot}}{M} \right)^{5/4} \left(\frac{R}{10 \text{ km}} \right)^{23/4} \left(\frac{T}{10^9 \text{ K}} \right)^2 \text{ s}, \quad (26)$$

where P is the rotation period of the star. These time scales depend on both the angular velocity and the temperature, and the condition $\tau < 0$ defines the region in the space $\Omega - T$ where the mode is unstable. In order to cross the instability window, the star must be hot and be a fast rotator. Only NSs born with initial rotation periods in the interval $P_{\text{K}} - P_{\text{f}}$ are unstable. Here, $P_{\text{K}} \simeq 8.05(\pi G \rho)^{-1/2}$ is the Keplerian period below which matter is ejected from the equator (Friedman et al. 1989) and, for a canonical NS of mass $1.4 M_{\odot}$ and radius $R = 10$ km, $P_{\text{K}} \simeq 0.68$ ms. Using the relations above, the corresponding temperature at which the star enters its instability region is $\sim 6 \times 10^{10}$ K. When the star cools to a temperature $\sim 4 \times 10^9$ K, corresponding to a critical rotation period of 20.8 ms, the shear viscosity stabilizes the star. Thus, three main phases can be identified in the evolutionary path of the star. Initially, the amplitude of the r-mode undergoes a rapid exponential growth, on a time scale of the order of one minute, without significantly affecting the rotation of the star. In this regime, the linearized hydrodynamic equations are a good approximation. After a few minutes, the amplitude α becomes so large that the linear theory is insufficient to describe the evolution of the mode. Non-linear studies suggest that the amplitude “saturates,” halting the growth of the mode at some amplitude of order unity, although the details of these non-linear effects are as yet poorly understood. In this “saturation phase,” the amplitude is treated as a phenomenological constant parameter ($\alpha \leq 1$); gravitational waves carry away the angular momentum of the star at a rate $dJ/dt \propto \Omega^7$ while the star continues to gradually cool. This saturation phase is the most likely to be detected and lasts about $10^4 - 10^5$ s for a crusted NS and about $10^6 - 10^7$ s for a fluid star. As the star spins down, the gravitational radiation gets much weaker, viscous damping becomes stronger and the star enters its “decay phase” when r-modes are stabilized by viscosity and the mode amplitude slowly dies away.

For purposes of detection, the most important characteristics of the GW signature from r-modes are: i) at the first order in the angular velocity of the star, the r-mode frequency for $m = 2$ is $\nu_{\text{gw}} = 4\nu_{\text{rot}}/3$ (Eq. (28)); ii) the emission is connected with mass-current multipoles instead of

mass multipoles and the expected strain amplitude in the saturation phase, calculated for a polytropic equation of state with $N = 1$ ($P \propto \rho^2$) and for a canonical NS of $1.4 M_\odot$, is Andersson & Kokkotas (2001)

$$h(t) \simeq 9.2 \times 10^{-25} \alpha \left(\frac{20 \text{ Mpc}}{D} \right). \quad (27)$$

In order to estimate the expected S/N ratio, the usual matched-filtering approach is adopted, although it must be recognized that such a technique is unlikely to be possible for this kind of signal. In this case

$$\left(\frac{S}{N} \right)^2 = 4 \int_0^\infty \left(\frac{h_c}{h_n} \right)^2 dl g \nu, \quad (28)$$

where $h_n = [\nu S_n(\nu)]^{1/2}$ and h_c is the characteristic amplitude defined by

$$h_c = h(t) \left[\nu^2 \left| \frac{dt}{d\nu} \right| \right]^{1/2}. \quad (29)$$

This last relation is a consequence of the stationary phase approximation, meaning that the detectability of a quasi-periodic signal is improved as the square root of the number of cycles at a given frequency ν increases. Under these conditions, for S/N=7, the maximum distances probed by VIRGO and LIGO are 0.54α Mpc and 0.40α Mpc respectively. For the planned EGO which requires the same S/N ratio, the maximum distance is about 23α Mpc.

An estimate of the expected number of events requires a previous estimate of the fraction of NSs born within the instability window. Performing a similar analysis as in the preceding section, one obtains $\zeta_r \simeq 1.7 \times 10^{-3}$. Using the local rate by Cappellaro et al. (1999), the expected rate of type II supernovae within the volume probed by EGO is 6.4 yr^{-1} and multiplying by the fraction ζ_r , one obtains a rate of one event every 92 yr.

Besides the rather low expected event rates, the relevance of r-modes is still in doubt, since they also face other difficulties. First, the r-mode instability might not be confirmed after all complicated physical processes that occur in NSs are taken into account. Second, the amount of angular momentum removed from the star and the strength of the GWs depend critically on the maximum amplitude α that can be reached by the r-mode, which might be limited by magnetic field effects (Rezzola et al. 2001) or by the leakage of energy to other damped modes by way of nonlinear couplings. Some of these issues have been investigated within a Newtonian framework by Lindblom et al. (2001). The picture which emerged from these simulations is quite different from that described above. The r-mode spin-down phase is faster (only a few minutes) and the frequency of GWs remains remarkably constant as the angular velocity of the star decreases. Even after the emission of GWs, the star continues to lose energy. This energy loss is probably related to density perturbations proportional to Y_{32}^B , which appear as waves with four crests (two in each hemisphere) on the surface of the star. As the amplitude reaches its maximum, these propagating crests turn into large, breaking waves, and the edges of the waves develop strong shocks that dump kinetic energy into thermal energy, thus killing the r-mode (Vallisneri 2003).

3.4 Quasi-Radial Oscillations

The new field of asteroseismology provides a wealth of information about the interiors of stars. For NSs in particular, a large number of pulsation modes are possible, but they are very difficult to observe in the electromagnetic spectrum. However, the analysis of X-ray data on hyperflares associated with the soft gamma repeaters (SGRs) 1806–20 and 1900+14 revealed the presence of quasi-periodic oscillations respectively in the range 18–93 Hz and 28–155 Hz for these objects. These oscillations can be interpreted as toroidal modes (Watts & Strohmayer 2007), allowing an estimation of the crust

thickness. Horvath (2005) raised the possibility that oscillations could be generated in the cracking of a solid quark star and that a substantial fraction of the released energy could be emitted in the form of GWs. More recently, Traylor et al. (2007) examined LIGO data obtained around the hyperflare event of 2004 December 27 associated with SGR 1806–20, concluding that the energy released in the form of GWs was less than 7.7×10^{46} erg for the 92.5 Hz mode.

Since the exhaustive work by Cowling (1941) was published, the “classical” (non-relativistic) approach to identify the main stellar oscillation modes was based on the restoring force that influences the fluid motion. Well known modes are the high frequency pressure *p-modes* and the low frequency gravity *g-modes*. Pressure is the restoring force for p-modes and frequencies associated with these modes depend on the travel time for acoustic waves to cross the star. The fundamental p-mode, whose eigenfunction has no nodes in the star, is usually referred to as the *f-mode* and, for NSs, the related frequencies are in the range 1.0–2.5 kHz. The g-modes, restored by gravity, sensitively depend on the internal composition and temperature distribution throughout the star and have frequencies of a few hundred Hz. Other common fluid modes are the shear (s-mode), toroidal (t-mode) and interface (i-mode). The interplay of all these modes in a NS is quite complex, since these objects may have a solid crust and a fluid core. The modes *p* and *g* belong to the class of polar modes, but if the shear modulus in the crust is non-zero, axial modes should exist as well as i-modes associated with the interface between distinct phases of matter inside NSs. The Newtonian picture has significantly changed in the past decades thanks to relativistic calculations, which have shown the existence of purely spacetime modes, the gravitational wave modes (w-modes), which are not present in the Newtonian approach (Kokkotas & Schutz 1986; Kojima et al. 1995; Andersson et al. 1996). These w-modes arise because of the trapping of a GW by the spacetime curvature generated by the background density. The w-modes exist for both polar and axial perturbations since they do not depend on fluid perturbations and have frequencies above 7 kHz, damped on time scales shorter than one millisecond. Moreover, axial modes, which were thought not to exist for non-rotating stars, do exist (Chandrasekhar & Ferrari 1991), have a frequency spectrum similar to w-modes and emit as much energy in the form of GWs as oscillating BHs.

Radial modes, by their simplicity, have been the first to be extensively investigated since they can provide information about the interior of stars. However, only non-radial oscillations produce GWs and early calculations concentrated mainly on the fundamental mode, through which most of the mechanical energy of the star is radiated away (Thorne & Campolattaro 1967; Thorne 1969; Lindblom & Detweiler 1983; Kokkotas & Schutz 1992). Since pure radial modes do not emit GWs, these oscillations are essentially damped by viscous forces. However, the situation is quite different if the star rotates (Chau 1967); since the degeneracy in the index *m* is removed, prograde ($m < 0$) modes are now distinct from retrograde ($m > 0$) modes and a non-rotating *l*-mode is split into $2l + 1$ different modes (Stergioulas 2003). Moreover, rotation couples a polar *l*-term to an axial $l \pm 1$ term and the coupling to the $l + 1$ term is strongly favored over the coupling to the $l - 1$ term. Similar conclusions follow from the analysis of axial modes (Chandrasekhar & Ferrari 1991; Kojima 1992; Stergioulas & Friedman 1998). As a consequence of these rotational couplings, even the lowest ($l = 0$) quasi-radial mode may radiate gravitational waves.

In rotating stars, Quasi-Normal Modes (QNMs) have been studied mainly in the slow rotation limit, in the post-Newtonian and in the Cowling approximation, which takes into account fluid displacements and neglects metric perturbations. The solution of the fully relativistic perturbation equations for a rapidly rotating star is still a very challenging task (see, Stergioulas 2003 and references therein). Quasi-radial modes in rotating relativistic stars have been studied by Hartle & Friedman (1975) and by Datta et al. (1998) in the slow rotation approximation. Yoshida & Eriguchi (2001) analyzed quasi-radial modes of rapidly rotating stars in the Cowling approximation and found that intersections between quasi-radial and other axisymmetric modes can appear near the Keplerian limit. Vincent (2008), using a linear theory, including both fluid and metric perturbations, computed the fundamental and the first overtone frequencies of rapidly rotating neutron star models based on

“realistic” equations of state, characterized by different nuclear compressibilities. Non-perturbative approaches have been developed recently by Font et al. (2000, 2002) and Dimmelmeier et al. (2006), who have used a relativistic code able to solve the coupled set of Einstein equations and the general 3D relativistic hydrodynamic equations, to study the long-term dynamical evolution of neutron stars.

A major problem concerning the emission of gravitational waves by an oscillating NS is the absence of a convincing excitation mechanism. Once the solid crust is formed, stresses produced by strong magnetic fields and/or rotation will be present and will induce tectonic activity. In this case, the stored elastic energy can be released as a consequence of star-quakes, which may excite radial and non-radial modes. However, the maximum elastic energy that can be channeled into oscillation modes is likely to be on the order of 10^{45} erg, restricting the detection of gravitational waves produced by those modes to galactic objects (de Freitas Pacheco 1998). Other more promising mechanisms able to excite oscillations have been proposed, such as the delayed collapse of the object resulting from the merger of two neutron stars (Shibata 2000) or the quake induced by a phase transition in the core (Cheng & Dai 1998; Miniutti et al. 2003). The contraction of a neutron star, induced by a first order phase transition occurring in the core, is a possible scenario in which quasi-radial oscillations may be excited. Neutron stars in low-mass X-ray binaries are spun up by accreting matter from the companion. In this case, the neutron star may accrete an amount of mass $\Delta M \geq 0.5 M_{\odot}$ in a timescale of about 10^8 yr, becoming a massive millisecond pulsar and having a central density high enough for the nuclear matter to undergo a phase transition. In fact, data on some binary millisecond pulsars located in globular clusters indicate that the associated neutron stars have masses significantly higher than the canonical value of $1.4 M_{\odot}$ (Freire et al. 2008a,b). Examples of these phase transitions are the formation of a kaon condensate and the deconfinement of quarks (Glendenning 2000), which soften the equation of state and produce a mini-collapse of the star. Pion and kaon condensates are likely to appear at densities above $(6-7)n_0$ ($n_0 = 0.16 \text{ fm}^{-3}$ is the nuclear saturation density) (Brown et al. 1994; Waas et al. 1997). At these supra-nuclear densities, the deconfinement of quarks might also occur. Initially, the quark matter will be composed of two flavors, u , and d and, subsequently, of three flavors u , d and s , forming the so-called strange quark matter (SQM), expected to be more stable than non-strange quark matter (Witten 1984). Because of the high degeneracy of matter constituents, temperature effects can be neglected and the phase transition occurs at a well defined P_c accompanied by an energy density jump at the phase interface. Stability requires that the Seidov (1971) criterion, e.g., the energy density jump across the transition surface, must satisfy the condition

$$\frac{\varepsilon_q}{\varepsilon_H} < \frac{3}{2} \left(1 + \frac{P_c}{\varepsilon_H} \right), \quad (30)$$

where ε_q and ε_H are respectively the energy densities of quark and hadron matter at the transition surface. A first-order phase transition allows for a metastability of the hadron phase for $P > P_c$. Thus, a metastable core could form during the NS evolution in which the central pressure increases due either to spin-down or accretion. In the metastable core, quarks can appear through a nucleation process leading to the formation of quark droplets inside the hadron matter. The energy barrier resulting from the surface tension at the quark-hadron interface delays the nucleation process until the pressure reaches a critical value at which the energy barrier vanishes. Above such a critical pressure, the core becomes unstable and converts immediately into the quark phase. The formation of a quark core (as well as the formation of a pion/kaon condensate) softens the equation of state, reducing the maximum stable mass and rendering the star unstable. Under these conditions, the NS may undergo a “mini-collapse” and the energy difference between the initial and the final star configuration is transformed into heat and/or mechanical energy in the form of oscillations, damped either by viscous forces or by the emission of GWs (Marranghello et al. 2002; Zdunik et al. 2006). It is worth mentioning that some authors have considered the excitation of the quadrupole mode during the the birth of a pure quark-star as a possible GW emission mechanism (Xu 2006). The same author,

assuming that millisecond pulsars are wobbling quark stars, estimated upper limits for their radius and mass using recent LIGO data.

The dynamics of the collapse induced by the hadron-quark phase transition was investigated by Lin et al. (2006), who performed simulations using a 3D Newtonian hydrodynamic code. They assumed the existence of an initial seed of SQM inside the core of the NS and that the conversion process occurs in a time scale much shorter than the dynamical time scale. At the end, the star has a core constituted by a mixed phase of nuclear and quark matter surrounded by a mantle of normal nuclear matter. Their “reference” model has a baryonic mass of $2.2 M_{\odot}$, a rotation period of 1.2 ms and an equatorial radius of 17.95 km. The resulting waveform is composed by two main modes: a quasi-radial mode of frequency 2.82 kHz and a quadrupole mode of frequency 2.08 kHz. The damping of the oscillations is of the order of a few milliseconds and is due essentially to the growth of the differential rotation and dissipation by strong shock waves. More recently, Abdikamalov et al. (2009) performed 2D relativistic calculations on the dynamics of the collapse also based on a polytropic equation of state, concluding that the observed damping by Lin et al. (2006) is probably dominated by numerical effects and is not due to the transfer of energy to rotation. Moreover, they conclude that the total energy emitted in the form of gravitational waves is considerably less than the values derived by Lin et al. (2006).

Stars, in these simulations of the collapse induced by a core phase transition, were modeled by assuming a polytropic equation of state, which explains the relatively high oscillation frequencies derived for the quasi-radial mode in spite that the considered star is quite massive. However, it is worth mentioning that the relativistic treatment by Abdikamalov et al. (2009) gives lower frequencies than those computed by Lin et al. (2006) for models of similar masses. In fact, for neutron star models built with “realistic” equations of state, one should expect that the quasi-radial mode frequencies decrease as the mass (or the central energy density) increases (Vincent 2008). Vincent & de Freitas Pacheco (2010) built a sequence of hadronic rotating neutron stars having a fixed baryonic mass ($1.965 M_{\odot}$), based on a “realistic” equation of state describing interactions in non-symmetric nuclear matter constituted by neutrons, protons, hyperons and leptons. Sequences of rotating hybrid models, including a quark core were also computed, based on the equation of state of deconfined matter given by de Freitas Pacheco (1999). As the rotation of the hadronic star decreases, the central density increases until the critical value for deconfinement is reached, corresponding to a pressure of $0.422 \text{ GeV fm}^{-3}$. At this point, the rotation period of the star is 2.16 ms, its equatorial radius is 10.29 km and its gravitational mass is $2.30 M_{\odot}$. Once the transition point is attained, the star suffers a small collapse, forming a core of deconfined matter having a mass of $\sim 7.8 \times 10^{-4} M_{\odot}$ and a radius of only 0.253 km. The total (equatorial) radius of the hybrid star is now 10.18 km, indicating that the star has shrunk by about 110 m! The variation of the gravitational mass corresponds to an energy release of approximately 2×10^{52} erg. The frequency of the quasi-radial mode at the moment of the transition is 510 Hz for the hadronic phase and 670 Hz for the hybrid phase. Notice that the expected oscillation frequency is considerable smaller than those predicted from polytropic models, being closer to the maximum sensibility of ground based laser interferometers.

Table 2 compares the main properties of the resulting hybrid models of similar rest mass computed by Vincent & de Freitas Pacheco (2010) and Abdikamalov et al. (2009). In Table 2, the first

Table 2 Comparison of the physical parameters of hybrid stars: model A1 by Abdikamalov et al. (2009) and HY2 by Vincent & de Freitas Pacheco (2010).

Model	$M_0 (M_{\odot})$	$M_g (M_{\odot})$	F (Hz)	P (ms)
A1	1.980	1.810	870	1.00
HY2	1.965	1.804	670	2.16

column identifies the model, the second gives the rest mass, the third gives the gravitational mass and the last two columns give respectively the frequency of the quasi-radial mode and the rotation period.

Supposing that the waveform of the quasi-radial mode is approximately given by a damped sinusoid, the signal-to-noise ratio for a matched-filtering of the signal is given by Equation (6). In this case, the wave amplitude is related to the energy E_{gw} released under the form of gravitational waves by

$$h_0 = \frac{2}{\pi D \nu_{\text{gw}}} \sqrt{\frac{G E_{\text{gw}}}{\tau_{\text{gw}} c^3}}, \quad (31)$$

where D is the distance to the source, ν_{gw} is the gravitational wave frequency and τ_{gw} is the damping timescale. When the quality factor of the oscillation $Q = \pi \nu \tau$ is greater than one (the present case), the maximum distance that a source can be detected for a given S/N ratio does not depend on the damping timescale. Combining the equation above for the amplitude with Equation (6), one obtains

$$D_{\text{max}} = \frac{9.43 \times 10^{-21}}{\nu_{\text{gw}}} \sqrt{\frac{E_{50}}{S_n(\nu_{\text{gw}})}}, \quad (32)$$

where E_{50} is the energy released in the form of gravitational waves in units of 10^{50} erg and the numerical factor was calculated for a signal-to-noise ratio $S/N=5$.

The fraction of the released energy which is channeled into gravitational radiation is still quite uncertain. According to the computations by Bhattacharyya et al. (2006), the deconfinement occurs in two distinct steps: in the first step, hadrons are converted in two-flavor (u, d) matter, quite a fast process with a timescale of about 1ms. In the second step, the weak interaction reaction $u+d \leftrightarrow u+s$ takes place converting the quark matter in “strange” matter. This reaction is quite slow and the core conversion into “strange” matter takes tens to hundreds of seconds, depending on the mass of the deconfined core. In this situation, one should expect that most of the released energy will be radiated. The Newtonian calculations by Lin et al. (2006) suggest that only 10% of the released energy is radiated away while the relativistic computations by Abdikamalov et al. (2009) indicate still lower values, i.e., approximately 0.034% of the released energy is emitted in the form of gravitational waves. If the latter estimates are correct, then even with advanced detectors, only galactic sources or those located in M31 could be detected. An “optimistic” estimate can be obtained assuming that most of the released energy is radiated and that the quasi-radial mode carries a similar energy as the quadrupole mode. In this case, from the model by Vicent & de Freitas Pacheco (2010), advanced-Ligo would be able to detect a signal up to a distance of 15 Mpc while EGO would see sources up to 100 Mpc, corresponding to an event rate of about one detection every 3–4 yr if the specific rate is about 10^{-5} yr^{-1} (Fryer et al. 1999; Pfahl et al. 2003).

4 BINARY SYSTEMS

4.1 NS-NS Binaries

The merger of two compact objects (NS-NS, BH-BH, NS-BH) are among the most important sources of GWs, since a huge amount of energy is released in the process. In particular, the coalescence of NS-NS binaries may radiate about 10^{53} erg in the last seconds of their inspiral trajectory, at frequencies up to 1.4–1.6 kHz, the range covered by most of the ground-based interferometers. To understand the process dynamics, the prediction of its signal waveform, the released power and the event rate, many theoretical investigations have been performed in the past years.

The dynamics of the inspiral and, in particular, the study of tidal effects in the very last orbits of an NS-NS system may put strong constraints on the equation of state of dense matter. Rosswog et al. (2000) performed 3D Newtonian hydrodynamic calculations of the last stages of the inspiral and

of the final coalescence of an NS-NS binary system, constituted by stars having masses of $1.3 M_{\odot}$ and $1.4 M_{\odot}$. Almost immediately after contact, a fast rotating massive central object is formed, with a mass above $2.3 M_{\odot}$. From the simulations by Rosswog et al., it is not possible to decide the fate of the central object. It might collapse to a BH, but also the formation of a supermassive NS with $\sim 2.7 M_{\odot}$ cannot completely be excluded. In the case of a larger mass difference between the components, the less massive star gets disrupted and engulfs the other object, that stays rather unaffected by the process. A fraction of the mass of the disrupted star is lost and the amount of ejected material depends on the adopted equation of state, whereas a thick disk containing between $0.051 M_{\odot}$ and $0.23 M_{\odot}$ forms around the central star. Full relativistic 3D simulations of the merger of two NSs were performed by Shibata et al. (2005) in a restricted mass ratio range ($0.9 \leq q \leq 1$). These simulations suggest that if the total mass of the system is larger than ~ 2.5 – $2.7 M_{\odot}$ (depending on the adopted equation of state), a BH is promptly formed irrespective of the initial mass ratio. In the other case, the outcome is a hypermassive NS of large ellipticity. According to the simulations by Shibata et al. (2005), in the formation of the hypermassive NS, quasiperiodic gravitational waves of a large amplitude and with frequencies in the range 3–4 kHz are emitted. The emission time scale is typically around 100 ms, after which the star collapses to a BH.

The coalescence of a system consisting of a BH and an NS was simulated by Lee (2000) using Newtonian hydrodynamics. The final inspiral phases were followed up to separations on the order of the stellar radius. For an equation of state with an adiabatic index $\gamma = d \log P / d \log \rho = 3$, after an initial phase of intense mass transfer, the NS is not completely disrupted and a remnant core remains in orbit around the BH in a stable binary configuration. For $\gamma = 2.5$, the tidal disruption process is more complex. The core of the NS survives the initial phase of mass transfer, but is totally disrupted during the next periastron passage. The resulting accretion disc formed around the BH contains a few tenths of a solar mass. The estimated efficiency $\varepsilon = (E/M_{\text{tot}}c^2)$ of the gravitational wave emission is typically $\sim 3.3 \times 10^{-3}$. Simulations in the framework of the GRT were performed by Faber et al. (2006), who considered the merger of an NS with a Schwarzschild BH. The results obtained by Faber et al. (2006) indicate that the mass transfer begins when the NS orbit is still outside the innermost stable orbit and is more unstable than expected by some crude analytical studies. This mass loss process is the driving mechanism determining the subsequent evolution of the orbit. The NS is disrupted after a few orbital periods and most of the mass transferred onto the BH is promptly accreted, but a fraction of about 30% of the mass is shed outward and finally ejected from the system.

If these simulations are now giving a more consistent scenario for the last evolutionary phases of the merging of two NSs or an NS and a BH, there is still some tension concerning the expected event rates.

Theoretical evaluations of the coalescence rate of NS-NS binaries are always performed in two main steps: firstly, the merging rate in our Galaxy is estimated and then, assuming that this rate is typical, an estimate is performed for the volume of the universe sampled by a given detector, using some adequate scaling. The galactic merging rate has been estimated either by using binary population synthesis models (Potergies-Zwart & Spreew 1996; Potergies-Zwart & Yungelson 1998; Belczynski et al. 2002) or from the statistics of the observed NS-NS binaries (Phinney 1991; van den Heuvel & Lorimer 1996; Kalogera et al. 2001; Kalogera et al. 2002; Kim et al. 2003). These estimates may differ by one order of magnitude, ranging in general from 10^{-6} yr^{-1} up to a few times 10^{-5} yr^{-1} , but values as high as $3 \times 10^{-4} \text{ yr}^{-1}$ have been reported in the literature (Tutukov & Yungelson 1993; Lipunov et al. 1997). Once the present galactic merging rate has been evaluated, the expected detection rate can be estimated by scaling the total luminosity within the volume probed by the detector with respect to the luminosity of the Galaxy at the same wave-band. Within the local universe ($z < 0.01$), the distribution of galaxies is not homogeneous and if the actual distribution is not taken into account, the expected detection rate may be seriously underestimated. For instance, the inclusion of the huge concentration of galaxies in the direction of Norma-Centaurus (the “Great Attractor”) may considerably increase the detection rate of these events (de Freitas Pacheco 1977).

Let $R_*(t)$ be the star formation rate (in $M_\odot \text{ yr}^{-1}$) and $P(\tau)$ be the probability per unit of disrupted time for a newly formed NS-NS binary to coalesce in a time scale τ . Under these conditions, the coalescence rate of NS-NS pairs at instant t in a given galaxy is

$$\nu_c(t) = f_b \beta_{\text{ns}} \lambda \int_{\tau_0}^{t-\tau_*-\tau_0} P(\tau) R_*(t - \tau_* - \tau) d\tau, \quad (33)$$

where f_b is the fraction of massive binaries formed among all stars, β_{ns} is the fraction of formed binaries which remain bounded after the second supernova event and $\lambda = 5.7 \times 10^{-3} M_\odot^{-1}$ is the fraction per unit mass of formed stars in the mass interval 9–40 M_\odot ; a Salpeter initial mass function was adopted. The mean evolutionary time scale required for the system to evolve into two neutron stars is τ_* , typically on the order of $10^7 - 10^8$ yr, whereas τ_0 is the minimum time scale required for an NS-NS binary to coalesce. According to the simulations reported by de Freitas Pacheco et al. (2006a), $\tau_0 \simeq 2 \times 10^5$ yr. From the aforementioned simulations, the authors derived for the coalescence probability, $P(\tau) = 0.087/\tau$, normalized in the interval $\tau_0 = 20$ Gyr, $\beta_{\text{ns}} = 0.024$ and $f_b = 0.136$. The fraction β_{ns} of bound binaries depends on the natal kick imparted to the nascent NS. Natal kicks may unbind binaries which otherwise might have remained bound or, less probable, conserve bound systems which without the kick would have been disassociated. Recent investigations on the spin period-eccentricity relation for NS-NS systems (Dewi et al. 2005) indicate that such a correlation can only be obtained if the second NS receives a kick substantially smaller than those commonly assumed for single radio pulsars, supporting the fact that de Freitas Pacheco et al. (2006a) assumed a natal kick velocity distribution with a 1D velocity distribution of about 80 km s^{-1} . Using the galactic star formation rate derived from observations (Rocha-Pinto et al. 2000), the present galactic NS-NS coalescence rate is $\nu_S = (1.7 \pm 1.0) \times 10^{-5} \text{ yr}^{-1}$.

Elliptical galaxies also contribute to the morphological composition of galaxies in the local universe. However, excluding the Milky Way, no direct information is available for the NS population and the star formation history for other galaxies. Thus, the coalescence rate in extragalactic objects can only theoretically be estimated. Assuming for a typical E-galaxy the model 3 by Idiart et al. (2003), and the same parameters f_b and β_{ns} derived for the Galaxy, de Freitas Pacheco et al. (2006a) estimated a present coalescence rate of $\nu_E = 8.6 \times 10^{-5} \text{ yr}^{-1}$. Adopting fractions of 35% and 65% respectively for ellipticals and spirals within the local universe, the result for the mean weighted coalescence rate is $\nu_c = 3.4 \times 10^{-5} \text{ yr}^{-1}$. The coalescence rate within a volume of radius D can now be estimated by using the scale factor $K(< D)$, defined by the ratio between the total B-luminosity within the considered volume, derived from LEDA, and the Milky Way B-luminosity. Figure 2, taken from de Freitas Pacheco et al. (2006a), shows the resulting coalescence rate within a volume of radius D .

The strength of a given signal is characterized by the S/N ratio, which depends on the source power spectrum and on the noise spectral density $S_n(\nu)$ of the detector. For the merging of NS-NS pairs, the optimum S/N ratio is obtained by the matched-filtering technique, e.g.,

$$\left(\frac{S}{N}\right)^2 = 4 \int_0^\infty \frac{|\tilde{h}(\nu)|^2}{S_n(\nu)} d\nu, \quad (34)$$

where $|\tilde{h}(\nu)|^2$ is the sum of the square of the Fourier transform of both polarization components. Following the approach by Finn (1996), the equation above can be recast as

$$\frac{S}{N} = 8\Theta \left(\frac{r_0}{D}\right) \left(\frac{\mathcal{M}}{1.2M_\odot}\right)^{5/6} \zeta(\nu_{\text{max}}), \quad (35)$$

where $D = (1+z)r$ is the luminosity distance to the source and the parameter r_0 is given by the relation

$$r_0 = 9.25 \times 10^{-22} \sqrt{I_{7/3}} \text{Mpc}, \quad (36)$$

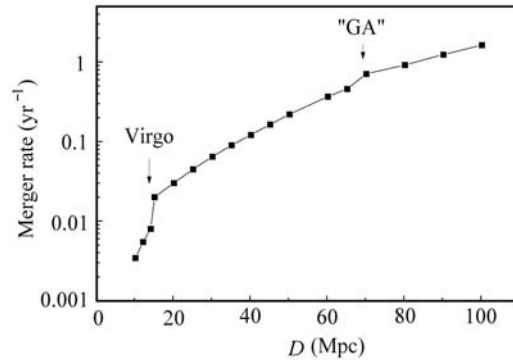


Fig. 2 Total expected NS-NS coalescence rate within a volume of radius D . The positions of the Virgo cluster and of the super-cluster dubbed. The Great Attractor are also indicated.

with

$$I_{7/3} = \left(\frac{\nu_{\odot}}{\pi}\right)^{1/3} \int_0^{\infty} \frac{d\nu}{\nu^{7/3} S_n(\nu)}, \quad (37)$$

where $\nu_{\odot} = 202.38$ kHz. The term $\zeta(\nu_{\max})$ is defined by the equation

$$\zeta(\nu_{\max}) = \frac{(\nu_{\odot}/\pi)^{1/3}}{I_{7/3}} \int_0^{2\nu_{\max}} \frac{d\nu}{\nu^{7/3} S_n(\nu)}. \quad (38)$$

The inspiral phase ends when the pair separation is such that tidal effects disrupt the stars or when the last stable orbit is reached, corresponding to a maximum orbital frequency $\nu_{\max} \sim 750$ Hz. The other parameter in Equation (45) is the chirp mass $\mathcal{M} = \mu^{3/5} M^{2/5}$, with μ and M being respectively the reduced and the total mass of the system. The angular function Θ depends on geometrical projection factors of the detector and on the inclination angle i between the orbital angular momentum of the binary and the line of sight, namely

$$\Theta^2 = 4 [(1 + \cos^2 i)^2 F_+^2 + 4 \cos^2 i F_{\times}^2]. \quad (39)$$

According to Finn & Chernoff (1993), the probability distribution of Θ can be approximated with quite a good accuracy by the relation

$$P(\Theta) = \frac{5\Theta(4 - \Theta)^3}{256} \quad \text{if } 0 \leq \Theta \leq 4. \quad (40)$$

From these equations, for a given S/N ratio and detector sensibility, the maximum distance probed by the instrument can be evaluated. Under these conditions, the parameter r_0 is 7.6 Mpc for VIRGO, 8.0 Mpc for LIGO and 120 Mpc for advanced-LIGO. Adopting S/N=7.0, the typical threshold for a false alarm rate of about one per year; the maximum probed distances are 13, 14 and 207 Mpc for VIRGO, LIGO and advanced-LIGO respectively. Using data from Figure 2, the mean expected event rates are one each 125 yr for LIGO, one each 148 yr for VIRGO and 6 events yr^{-1} for advanced-LIGO.

Spallicci (2003) and Spallicci et al. (2005) analyzed the spectral noise density of VIRGO in the context of chirp signal detection. These studies suggest that the reduction of the mirror thermal noise may provide the highest gain in the S/N ratio. The direct dependence of the mirror thermal noise power spectrum on the temperature points to the use of already existing cryogenic techniques.

In parallel, also the pendulum thermal and shot noise should be reduced in such a frequency band. If the mirror thermal noise is reduced by a factor of 10, a gain by a factor of 8 can be obtained, increasing the maximum distance probed by VIRGO up to 110 Mpc and allowing an expected detection rate of about 3 events every 2 yr. These results suggest that only the planned sensibility of advanced interferometers will permit researchers to probe the local universe deep enough for at least a few events to be seen during a monitoring period of 1–2 yr. An alternative strategy for the present (and future) generation of laser interferometers is the search of these events by using a network of detectors, since for a given false alarm rate, the detection threshold is lowered as the number of detectors increases. Data analysis of chirp signals detected by a network of gravitational antennas, in particular that constituted by the two LIGO (Hanford and Livingston) and VIRGO detectors was recently considered by Pai et al. (2002). Those authors estimated the increased detection sensibility for such a combination of detectors and, for a false alarm rate equal to one per year and a detection probability of 95%, the maximum probed distance turns out to be around 22 Mpc, corresponding to an event rate of about one every 26 yr and implying a gain of a factor of 5 with respect to a single interferometer.

4.2 BH-BH Binaries

Investigations on binary systems consisting either of two BHs or a BH and an NS have received great attention in the past years, in particular because of effects from the spin-orbit interaction. The detection of binary BHs in laser interferometer data requires adequate waveform templates and therefore, an accurate knowledge of the orbital evolution. Three regimes in the inspiral motion can be recognized: *a*) the *adiabatic regime*, in which the two bodies gradually approach each other through a sequence of quasi-circular geodesic orbits; *b*) the *transition regime*, near the innermost stable circular orbit (ISCO) and *c*), the *plunge regime*, in which the compact star travels on a geodesic from slightly below the inner stable circular orbit into the BH's horizon or, when the system consists of two BHs, the two horizons merge.

Recently, re-summation techniques have made it possible to accelerate the convergence of asymptotic post-Newtonian series and derive waveforms beyond the adiabatic approximation (Damour et al. 2001). This approach permits the calculation of waveforms that extends beyond the inspiral regime into the plunge phase, followed by the quasi-normal mode ringing. Baker et al. (2001) used a technique that combines the full numerical approach to solve Einstein equations, applied in the true non-linear regime, and linearized perturbation theory around the final distorted single BH at later times. They have also computed plunge waveforms, which show a nonnegligible signal lasting for over $100 GM c^{-3}$. For a system with a total mass of $35 M_{\odot}$, a frequency decomposition of the waveform shows two dominant components at 600 Hz and 900 Hz, which are close to the most weakly damped quasi-normal modes $m = \pm 2$. Baker et al. (2001) estimated that the total radiated GW energy after ISCO is about 4%–5% of the total mass, coming almost entirely from the $m = \pm 2$ modes and larger than the estimates by Buonanno & Damour (2000). The upper bound on the amount of angular momentum lost in the event is around 0.1%, confirming early expectations that not much angular momentum is lost during the plunge and ring-down.

Concerning estimates of the expected event rate, the situation is still more uncertain than the merging rate of two NSs. Theoretical studies have been carried out most often via population synthesis methods, that allow for a self-consistent evolution of massive stars leading to the formation of different populations of compact objects. Extensive calculations have been performed by Belczynsky et al. (2006 and references therein) on population synthesis of compact star binaries. Their reference model predicts a galactic merger rate for NS-NS binaries of $(1.2 - 1.9) \times 10^{-5} \text{ yr}^{-1}$, in quite good agreement with the results of de Freitas Pacheco et al. (2006a) reported in the previous section. The model by Belczynsky et al. (2006) also predicts a galactic merger rate of $(7 - 11) \times 10^{-8} \text{ yr}^{-1}$ for NS-BH binaries and of $(2.0 - 3.0) \times 10^{-8} \text{ yr}^{-1}$ for BH-BH binaries.

The expected event rate can be estimated by using the same procedure developed in the previous section and using the above merger rates. Assuming that BH-BH binaries are constituted by two objects of $9 M_{\odot}$, the maximum distances probed by VIRGO and LIGO are respectively 48 Mpc and 52 Mpc, corresponding to an expected rate of about one event every 6 000 yr. For advanced LIGO, the maximum probed distance is ~ 820 Mpc and one event every 3.6 yr is expected, while for EGO the predicted rate is about 54 times higher, e.g., 15 events yr^{-1} (these estimates for the theoretical event rates suppose a $S/N = 7$).

4.3 Supermassive Black Holes and Compact Stars

Presently, there is a general consensus that most, if not all, galaxies host supermassive black holes (SMBHs) with masses ranging from $\sim 10^6 M_{\odot}$ up to a few $10^9 M_{\odot}$. These SMBHs are generally embedded in dense stellar environments and, consequently, they may capture stars which either will promptly be swallowed through the horizon or will inspiral by emitting GWs. Interactions between stars and SMBHs in dense galactic nuclei have been the focus of many investigations in the past years, since these events are potential sources for the space mission LISA.

The planned LISA noise spectral density is minimized around frequencies $\sim (3 - 30)$ mHz, setting the BH mass interval of interest in the range $\sim 10^5$ up to a few $\times 10^6 M_{\odot}$. Main sequence stars, which dominate a given stellar population, will be disrupted by tidal forces if the BH mass is less than $\sim 2 \times 10^8 M_{\odot}$, since the Roche limit will be inside their gravitational radius. Thus, only the capture of compact objects like white dwarfs (WDs), neutron stars and stellar mass black holes may produce a gravitational signal relevant for LISA.

Because of the complexity of the energy and angular momentum transfer during stellar encounters inside the influence sphere, a region where the orbits are dominated by the gravitational potential of the central BH, predicted capture rates may vary by orders of magnitude. An early Monte Carlo simulation of the stellar random walk in J-space was performed by Hills & Bender (1995), using parameters appropriate for the core of the dwarf elliptical M32, resulting in a capture rate of $1.9 \times 10^{-8} \text{ yr}^{-1}$, if compact stars are assumed to represent 10% of the total stellar population. Similar simulations were performed by Freitag (2003) but for parameters appropriate to the galactic center. In this case, the capture rate of WDs was found to be $\sim (2 - 3) \times 10^{-7} \text{ yr}^{-1}$ and those of NSs and BHs about one order of magnitude lower. Analytical estimates of the capture rate were performed by Sigurdsson & Rees (1997), who have found, in particular for M32, a rate comparable to that obtained by Hills & Bender (1995). Analytical and Monte Carlo methods were adopted by Hopman & Alexander (2005) and from their approach a typical event rate of a few $\times 10^{-9} \text{ yr}^{-1}$ per galaxy was derived. If coherent interactions are taken into account, capture rates can be enhanced up to one order of magnitude in comparison with a current of stars driven only by non resonant relaxation (Hopman & Alexander 2006).

Estimates of capture rates including resonant and non resonant relaxation effects were performed by de Freitas Pacheco et al. (2006b). The stellar density in the influence sphere was estimated from brightness profiles derived from Hubble Space Telescope observations (Faber et al. 1997) and the fraction of compact objects as a function of the galaxy's luminosity was derived from an upgraded version of the evolutionary models developed by Idiart et al. (2003). The derived WD capture rate as a function of the SMBH mass is

$$R_{\text{wd}} = \frac{0.86}{(M_{\text{bh}}/M_{\odot})^{1.048}} \text{ yr}^{-1}. \quad (41)$$

In the first approximation, the capture rate of NSs and BHs can be obtained by multiplying the equation above by 0.0511 and 0.00916 respectively.

The number of events expected to be detected by LISA demands a previous evaluation of the volume of the universe probed by the detector or, in other words, an evaluation of the maximum

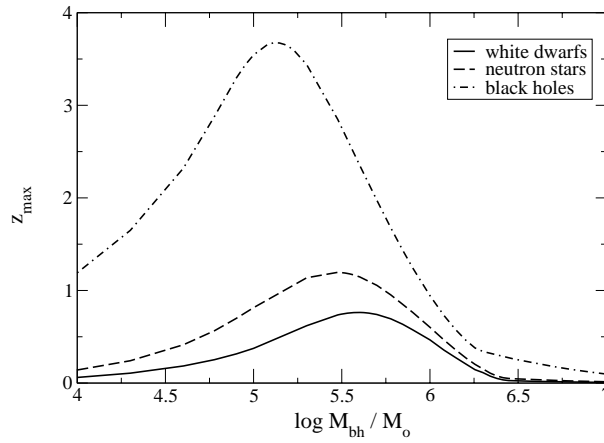


Fig. 3 Maximum redshift at which a gravitational signal resulting from an inspiral capture can be detected by LISA operating as a Michelson interferometer. An $S/N=5$ was adopted and the WD-WD galactic binary confusion noise was included. Typical masses, $m_{\text{wd}} = 0.7 M_{\odot}$, $m_{\text{ns}} = 1.4 M_{\odot}$ and $m_{\text{bh}} = 10 M_{\odot}$ were adopted in the calculations. Adapted from de Freitas Pacheco et al. (2006b).

redshift at which a given inspiral gravitational signal can be seen. For the inspiral up to the last stable orbit, theoretical templates of the waveform will probably be available and the method of matched filtering can be used. In this case, averaging over source positions and orientations, the resulting S/N ratio is (Cornish 2001)

$$\left(\frac{S}{N}\right)^2 = 2 \int_0^{\infty} \frac{S_h(\nu)R(\nu)}{S_n(\nu)} d\nu, \quad (42)$$

where $R(\nu)$ is the response function of the detector averaged over all sky directions and polarizations and $|\tilde{h}(\nu)|^2 = S_h(\nu)R(\nu)$. Using the spectral density of the gravitational signal derived from the quadrupole approximation, which is adequate to estimate the signal-to-noise ratio, and setting $S/N=5$, the value adopted in the LISA community, the maximum redshift as a function of the SMBH mass, for a given compact object mass, can be estimated.

Figure 3 shows the resulting curves for different compact objects and for cosmological parameters $\Omega_{\Lambda} = 0.7$ and $\Omega_m = 0.3$. The farthest spiral signal resulting from the capture of a WD corresponds to a redshift $z_{\text{max}} \sim 0.76$ and an SMBH mass of about $3.9 \times 10^5 M_{\odot}$, that resulting from the capture of an NS corresponds to $z_{\text{max}} \sim 1.2$ and an SMBH of $3.1 \times 10^5 M_{\odot}$ whereas the signal resulting from the capture of a stellar BH by an SMBH of mass $1.3 \times 10^5 M_{\odot}$ can be seen up to $z \sim 3.7$.

Once the maximum redshift at which a given inspiral signal can be detected is known, the expected number of events Γ in a time interval T can be estimated from the equation

$$\Gamma = T \int_{M_1}^{M_2} \frac{R(M)}{(1+z)} \frac{d\mathcal{N}(M, z)}{dM} dM \int_0^{z(M)} \frac{dV}{dz} dz. \quad (43)$$

In this equation, $R(M)$ is the capture rate of a given compact object as a function of the SMBH mass; the term $(1+z)$ in the denominator corrects for the time dilation and $d\mathcal{N}(M, z)/dM$ is the SMBH mass distribution taken from Aller & Richstone (2002). The upper limit M_2 in the second integral corresponds to the critical mass ($\simeq 8 \times 10^6 M_{\odot}$) beyond which the relaxation time is larger than

12 Gyr and, consequently, a steady stellar current cannot be established (de Freitas Pacheco et al. 2006b). The lower mass cutoff M_1 is uncertain since, up to the present time, observational searches for intermediate mass BHs have been discouraging. Presently, the smallest known central BH is located in the dwarf elliptical M32, having a mass $\sim 1.4 \times 10^6 M_\odot$. This leads to a conservative estimate of the number of events that can be obtained if this value is taken as the minimum mass. From an observational point of view, the existence of SMBHs with masses lower than such a limit is still controversial. Analyses of dynamical data on the dwarf galaxies M33 and NGC 205 lead to robust upper limits respectively of $\sim 3 \times 10^3 M_\odot$ and $\sim 4 \times 10^4 M_\odot$ for the putative BHs living in the center of these objects (Merrit et al. 2001; Gebhardt et al. 2001; Valluri et al. 2005). Moreover, searches for intermediate mass BHs in dwarf-spheroidal satellites of the Milky Way have also been negative (Maccarone et al. 2005). However, these small galaxies were captured by our Galaxy and, in the process, collective effects may transfer energy to their central BHs, enough to move them far away from the core, thus escaping detection. If direct dynamical evidences of SMBHs in such a mass range are missing, indirect signals of their presence in narrow-line Seyfert-1 nuclei exist. Using the line-width-luminosity-mass scaling relation established for broad-line AGNs, SMBH masses were estimated by Greene & Ho (2004) for a sample of 19 galaxies, all in the range 8×10^4 up to $8 \times 10^6 M_\odot$. An “optimistic” estimate can also be performed if the lower mass cutoff M_1 is extended down to $2 \times 10^5 M_\odot$, corresponding to host galaxies and bulges brighter than $M_B = -14$. Under these conditions, in the *conservative* case **9** inspiral events are expected to be detected by LISA. The estimated probability to have a WD capture is 84.5% and those for the capture of a NS or a stellar BH are 8.0% and 7.5% respectively. Early-type galaxies are expected to contribute to about 53.8% of the total number of events, *Sa+Sb* bulges contribute to about 26.9% and *Sc* bulges contribute to about 19.3%. If the lower mass integration limit is reduced down to $2 \times 10^5 M_\odot$, there is a dramatic increase in the expected number of events. This occurs because the capture rate increases for lower SMBH masses as well as the volume of the universe probed by LISA. In the *optimistic* case, the expected number of events is **579**. The contribution of the various compact objects is now rather different: stellar BHs are expected to represent about 47.4% of the total number of events, NSs will contribute to about 33.5% and WDs, to about 19.1%. The contribution of the different morphological types remains practically unchanged, e.g., *E+S0* will contribute to about 53.2%, *Sa+Sb*, to about 20.5% and *Sc* to about 26.3%.

5 FINAL CONCLUSIONS

The first direct detection of gravitational waves will constitute an extraordinary scientific accomplishment, which will give further support to the General Relativity Theory and will open a new window to explore the universe.

If detected, gravitational waves from oscillating neutron stars or from the very last phases of the coalescence of an NS-NS binary will yield major insights into the properties of nuclear matter. Moreover, the eventual detection of gravitational waves from the ring-down phase of a newly formed black hole will permit researchers to directly probe their properties like mass and angular momentum. The observed rate of these rare events will impose severe constraints on the last evolutionary phases of massive stars; the detection of the GW background produced by these sources will teach us about the star formation activity in the past history of the universe as well as the very early phases of the big-bang, when radiation and matter were still strongly coupled. A still more fascinating possibility is related to theories describing our world such as a brane embedded in a higher dimensional space, having the purpose of solving the huge energy gap that separates the electroweak scale from the Planck scale, the so-called hierarchy problem. In this scenario, gravitational waves are produced by coherently excited *radions* (with the geometric degree of freedom controlling the size or curvature of the extra dimensions) and Nambu-Goldstone modes. According to estimates by Hogan (2000), the typical gravitational wave frequency is 0.1 mHz (out of the frequency range

covered by ground-based interferometers) and the amplitude corresponds to an equivalent density parameter $\Omega \sim 8 \times 10^{-5}$.

Different investigations performed in the past years indicate that the present generation of ground-based interferometers does not have a sensitivity high enough to probe a large volume of the universe and, therefore, the predicted event rates are quite small. However, it is worth mentioning that most of our models are still in their infancy and a large number of (astrophysical) parameters required for modeling remains quite uncertain. Planned ground-based advanced detectors will probably detect, for the first time, a gravitational wave signal. The dynamics of the inspiral of two neutron stars down to the last stable orbit is well understood and different estimates of the galactic merging rate are now quite consistent. Therefore, the prediction of a few events per year (case of advanced-LIGO) seems to be reliable. The situation is similar for the merging of two stellar black holes. Our knowledge of the inspiral and plunge dynamics has considerably improved in the past years but merging rates are still uncertain by one order of magnitude. Nevertheless, even with such an uncertainty, the planned sensitivity of EGO is high enough to expect that 2–15 events per year would be seen. The physics of the bar-mode instability requires further investigations and, in particular, the gravitational wave emission during the evolution of the star in its secularly unstable phase. Predicted event rates depend not only on the sensitivity of the detector but also on the fraction of neutron stars born in the instability interval. Present models suggest that EGO will be able to detect one event every two years (comparable to the expected ring-down produced during BH formation, e.g., one event every 5.5 yr). These numbers should be taken cautiously because, besides uncertainties in the physics of the considered transition, the initial rotation period distribution within the instability window is still not well known.

In space, the sensitivity of LISA will be enough to detect, even within a “pessimistic” perspective, a few stellar captures per year by supermassive black holes. Studies performed a few decades ago have pointed out that close binary systems should be potential sources of low frequency ($\nu_{\text{gw}} < 0.1$ mHz) GWs and, thus, potential targets for LISA. However, more detailed analyses (Meliani et al. 2000) indicate that these binaries, in particular those belonging to the class of Cataclysmic Variables, are not above the “confusion noise” generated by all galactic binary systems.

Appendix A:

Fits for the sensitivity curves of advanced interferometers used in the estimates performed in the present work are given below. They are available and updated, as the different projects evolve, at the web site <http://carina.astro.cf.ac.uk/geo/advligo/>.

A.1. Advanced LIGO

$$S_n(x) = 10^{-49} \left[111 \frac{(1 - x^2 + x^4/2)}{(1 + x^2/2)} + x^{-4.14} - 5x^{-2} \right] \text{ Hz}^{-1}, \quad (\text{A.1})$$

where $x = \nu/\nu_0$ and $\nu_0 = 215$ Hz. This fit can be used in the frequency interval 10–6000 Hz.

A.2. EGO

$$S_n(x) = 1.62 \times 10^{-51} \left[x^{-4.05} + 185.62x^{-0.69} + 232.56 \frac{N(x)}{D(x)} \right] \text{ Hz}^{-1}, \quad (\text{A.2})$$

where $x = \nu/\nu_0$ and $\nu_0 = 200$ Hz. The functions $N(x)$ and $D(x)$ are defined respectively as

$$N(x) = 1 + 31.18x - 64.72x^2 + 52.24x^3 - 42.16x^4 + 10.17x^5 + 11.53x^6, \quad (\text{A.3})$$

and

$$D(x) = 1 + 13.58x - 36.46x^2 + 18.56x^3 + 27.43x^4. \quad (\text{A.4})$$

References

- Abbott, B., et al. 2007, *Phys. Rev. D*, 76, 042001
- Abdikamalov, E. B., Dimmelmeier, H., Rezzolla, L., & Miller, J. C. 2009, *MNRAS*, 392, 52
- Abramovici, A., et al. 1992, *Science*, 256, 325
- Aller, M. C., & Richstone, D. 2002, *AJ*, 124, 3035
- Andersson, N., Kokkotas, K. D., & Schultz, B. F. 1996, *MNRAS*, 280, 1230
- Andersson, N., & Kokkotas, K. D. 2001, *Int. J. Mod. Phys. D*, 10, 381
- Baker, J., Bruggmann, B., Campanelli, M., Lousto, C.O., & Takahashi, R. 2001, *Phys. Rev. Lett.*, 87, 121103
- Bhattacharyya, A., Ghosh, S., Joarder, P. S., Mallick, R., & Raha, S. 2006, *Phys. Rev. C*, 74, 065804
- Belczynski, K., Kalogera, V., & Bulik, T. 2002, *ApJ*, 572, 407
- Bildsten, L. 1998, *ApJ*, 501, L89
- Bonaldi, M., et al. 2003, *Phys. Rev. D*, 68, 102004
- Bonazzola, S., &ourgoulhon, E. 1996, *A&A*, 312, 675
- Bradaschia, C., et al. 1990, *Nucl. Instrum. Methods A*, 289, 518
- Brown, G., Lee, C., Rho, M., & Thorsson, V. 1994, *Nucl. Phys. A*, 567, 937
- Brown, J. D. 2000, *Phys. Rev. D*, 62, 084024
- Buonanno, A., & Damour, T. 2000, *Phys. Rev. D*, 62, 064015
- Burrows, A., & Hayes, J. 1996, *Phys. Rev. Lett.*, 76, 352
- Burrows, A., Livne, E., Dessart, L., Ott, C. D., & Murphy, J. 2007, *ApJ*, 655, 416
- Cappellaro, E., Evans, R., & Turatto, M. 1999, *A&A*, 351, 459
- Centrella, J. M., New, K. C. B., Lowe, L. L., & Brown, J. D. 2001, *ApJ*, 550, L193
- Cerdonio, M., Conti, L., Lobo, J. A., Ortolan, A., Taffarello, L., & Zendri, J. P. 2001, *Phys. Rev. Lett.*, 87, 031101
- Chandrasekhar, S., & Fermi, E. 1953, *ApJ*, 118, 116
- Chandrasekhar, S., & Ferrari, V. 1991, *Proc. R. Soc. Lond. A*, 434, 449
- Chau, W.-Y. 1967, *ApJ*, 147, 664
- Cheng, K. S., & Dai, Z. G. 1998, *ApJ*, 492, 281
- Cowling, T. G. 1941, *MNRAS*, 101, 367
- Cornish, N. J. 2001, *Phys. Rev. D*, 65, 022004
- Damour, T., Iyer, B. R., & Sathyaprakash, B. S. 2001, *Phys. Rev. D*, 63, 044023
- Datta, B., Hasan, S. S., Sahu, P. K., & Prasanna, A. R. 1998, *Int. J. Mod. Phys. D*, 7, 49
- de Freitas Pacheco, J. A. 1997, *Astropart. Phys.*, 8, 21
- de Freitas Pacheco, J. A. 1998, *A&A*, 336, 397
- de Freitas Pacheco, J. A. 1999, in *Structure and Stability of Nucleon and Nuclear Systems*, eds. A. A. Raduta, S. Stoica, & I. I. Irsu (Singapore: World Scientific), 547
- de Freitas Pacheco, J. A., Regimbau, T., Vincent, S., & Spallicci, A. 2006a, *Int. J. Mod. Phys. D*, 15, 235
- de Freitas Pacheco, J. A., Filloux, C., & Regimbau, T. 2006b, *Phys. Rev. D*, 74, 023001
- Dimmelmeier, H., Stergioulas, N., & Font, J. A. 2006, *MNRAS*, 368, 1609
- Dewi, J.D.M., Podsiadlowski, Ph., & Pols, O. R. 2005, *MNRAS*, 363, L71
- Echeverria, F. 1989, *Phys. Rev. D*, 40, 3194

- Faber, S., et al. 1997, *AJ*, 114, 1771
- Faber, J. A., Baumgarte, T. W., Shapiro, S. L., Taniguchi, K., & Rasio, F. A. 2006, *Phys. Rev. D*, 73, 024012
- Ferraro, V. C. A. 1954, *ApJ*, 119, 407
- Finn, L. S. 1996, *Phys. Rev. D*, 53, 2878
- Finn, L. S., & Chernoff, D. F. 1993, *Phys. Rev. D*, 47, 2198
- Font, J. A., Miller, M., Suen, W. M., & Tobias, M. 2000, *Phys. Rev. D*, 61, 044011
- Font, J. A., Goodale, T., Iyer, S., Miller, M., Rezzolla, L., Seidel, E., Stergioulas, N., Suen, W.-M., & Tobias, M. 2002, *Phys. Rev. D*, 65, 084024
- Freire, P. C. C., Ransom, S. M., Begin, S., Stairs, I. H., Hessels, J. W. T., Frey, L. H., & Camilo, F. 2008a, *ApJ*, 675, 670
- Freire, P. C. C., Wolszczan, A., van den Berg, M., & Hessels, J. W. T. 2008b, *ApJ*, 679, 1433
- Freitag, M. 2003, *ApJ*, 583, L21
- Friedman, J. L., Ipser, J. R., & Parker, L. 1989, *Phys. Rev. Lett.*, 62, 3015
- Fryer, C. L. 1999, *ApJ*, 522, 413
- Fryer, C. L., Benz, W., Colgate, S. A., & Herant, M. 1999, *ApJ*, 516, 892
- Gal'tsov, D. V., & Tsvetkov, V. P. 1984, *Phys. Lett. A*, 103, 193
- Gebhardt, K., et al. 2001, *AJ*, 122, 2469
- Glendenning, N. K. 2000, in *Compact Stars, Nuclear Physics, Particle Physics and General Relativity* (Berlin: Springer)
- Greene, J. E., & Ho, L. C. 2004, *ApJ*, 610, 722
- Hartle, J. B., & Friedman, J. L. 1975, *ApJ*, 196, 653
- Heger, A., Woosley, S. E., & Spruit, H. C. 2005, *ApJ*, 626, 350
- Heyl, J. S., & Kulkarny, S. R. 1998, *ApJ*, 506, L61
- Hills, D., & Bender, P. 1995, *ApJ*, 445, L7
- Hirschi, R., Meynet, G., & Maeder, A. 2004, *A&A*, 425, 649
- Hogan, C. J. 2000, *Phys. Rev. Lett.*, 85, 2044
- Hopkins, A. M., & Beacom, J. F. 2006, *ApJ*, 651, 142
- Hopman, C., & Alexander, T. 2005, *ApJ*, 629, 362
- Hopman, C., & Alexander, T. 2006, *ApJ*, 645, 1152
- Horowitz, C. J., & Kadau, K. 2009, *PRL*, 102, 191102
- Horvath, J. E. 2005, *Mod. Phys. Lett. A*, 20, 2799
- Houser, J. L., Centrella, J. M., & Smith, S. C. 1994, *Phys. Rev. Lett.*, 72, 1314
- Houser, J. L., & Centrella, J. M. 1996, *Phys. Rev. D*, 54, 7278
- Hulse, R. A., & Taylor, J. H. 1975, *ApJ*, 195, L51
- Idiart, T. P., Michard, R., & de Freitas Pacheco, J. A. 2003, *A&A*, 398, 949
- James, R. A. 1964, *ApJ*, 140, 552
- Jaranowski, P., Królak, A., & Schultz, B. F. 1998, *Phys. Rev. D*, 58, 063001
- Kalogera, V., Narayan, R., Spiegel, D. N., & Taylor, J. H. 2001, *ApJ*, 556, 340
- Kalogera, V., et al. 2002, *ApJ*, 601, L179
- Kaper, L., Lamers, H. J. G. L. M., Ruymaekers, E., van den Heuvel, E. P. J., & Zuiderwijk, E. J. 1995, *A&A*, 300, 446
- Kim, C., Kalogera, V., & Lorimer, D. R. 2003, *ApJ*, 584, 985
- Kojima, Y. 1992, *Phys. Rev. D*, 46, 4289
- Kojima, Y., Andersson, N., & Kokkotas, K. D. 1995, *Proc. R. Soc. Lond. A*, 451, 341
- Kokkotas, K. D., & Schultz, B. F. 1986, *General Relativity and Gravitation*, 18, 913
- Kokkotas, K. D., & Schultz, B. F. 1992, *MNRAS*, 255, 119
- Konno, K., Obata, T., & Kojima, Y. 1999, *A&A*, 352, 211
- Konno, K., Obata, T., & Kojima, Y. 2000, *A&A*, 356, 234

- Kotake, K., Ohnishi, N., & Yamada, S. 2007, *ApJ*, 655, 406
- Kouveliotou, C., et al. 1998, *Nature*, 393, 235
- Kouveliotou, C., et al. 1999, *ApJ*, 510, L115
- Kuroda, K., et al. 1997, *Proc. Int. Conf. on Gravitational Waves: Sources & Detectors*, eds. I. Ciufolini, & F. Fiducaro (Singapore: World Scientific), 1007
- Lai, D., & Shapiro, S. L. 1995, *ApJ*, 442, 259
- Lee, W. H. 2000, *MNRAS*, 318, 606
- Lin, L.-M., Cheng, K. S., Chu, M.-C., & Suen, W.-M. 2006, *ApJ*, 639, 382
- Lindblom, L., & Detweiler, S. L. 1983, *ApJS*, 553, 73
- Lindblom, L., Tohline, J., & Vallisneri, M. 2001, *Phys. Rev. Lett.*, 86, 1152 (see also *Phys. Rev. D*, 65, 084039, 2002)
- Lipunov, V. M., Postnov, K. A., & Prokhorov, M. E. 1997, *MNRAS*, 288, 245
- Liu, Y. T., & Lindblom, L. 2001, *MNRAS*, 324, 1063
- Loffler, F., Rezzolla, L., & Ansorg, M. 2006, *Phys. Rev. D*, 74, 104018
- Maccarone, T. J., Fender, R. P., & Tzioumis, A. K. 2005, *MNRAS*, 356, L17
- Marranghello, G. F., Vasconcellos, C. A. Z., & de Freitas Pacheco, J. A. 2002, *Phys. Rev. D*, 66, 064027
- Meliani, M. T., de Araújo, J. C. N., & Aguiar, O. D. 2000, *A&A*, 358, 417
- Mereghetti, S. 1999, *The Neutron Star-Black Hole Connexion*, NATO-ASI, 13 (arXiv:astro-ph/9911252)
- Merrit, D., Ferrarese, L., & Joseph, C. L. 2001, *Science*, 293, 1116
- Miniutti, G., Pons, J. A., Berti, E., Gualtieri, L., & Ferrari, V. 2003, *MNRAS*, 338, 389
- Morsink, S., Stergioulas, N., & Blattnig, S. 1999, *ApJ*, 510, 854
- Moss, G. E., Miller, L. R., & Forward, R. L. 1971, *Appl. Opt.*, 10, 2495
- Muller, E., & Janka, H.-T. 1997, *A&A*, 317, 140
- Muller, E., Rampp, M., Buras, R., Janka, H.-T., & Shoemaker, D. H. 2004, *ApJ*, 603, 221
- Muno, M. P., et al. 2005, *ApJ*, 636, L41
- Nagar, A., Diaz, G., Pons, J. A., & Font, J. A. 2004, *Phys. Rev. D*, 69, 124028
- Ostriker, J. P., & Gunn, J. E. 1969, *ApJ*, 157, 1395
- Ott, C. D., Burrows, A., Dessart, L., & Livne, E. 2006, *Phys. Rev. Lett.*, 96, 201102
- Owen, B. J. 2005, *Phys. Rev. Lett.*, 95, 211101
- Pai, A., Dhurandhar, S., & Bose, S. 2002, *Phys. Rev. D*, 64, 042004
- Palomba, C. 2001, *A&A*, 367, 525
- Papadopoulos, P., & Font, J. A. 2001, *Phys. Rev. D*, 63, 044016
- Pfahl, E., Rappaport, S., & Podsiadlowski, P. 2003, *ApJ*, 597, 1036
- Phinney, E. S. 1991, *ApJ*, 380, L17
- Potergies-Zwart, S. F., & Spreew, H. N. 1996, *A&A*, 312, 670
- Potergies-Zwart, S. F., & Yungelson, L. 1998, *A&A*, 332, 173
- Regimbau, T., & de Freitas Pacheco, J. A. 2000, *A&A*, 359, 242
- Regimbau, T., & de Freitas Pacheco, J. A. 2001, *A&A*, 374, 182
- Regimbau, T., & de Freitas Pacheco, J. A. 2003, *A&A*, 401, 385
- Regimbau, T., & de Freitas Pacheco, J. A. 2006, *A&A*, 447, 1
- Rezzola, L., Lamb, F. L., Markovic, D., & Shapiro, S. L. 2001, *Phys. Rev. D*, 64, 104013
- Rocha-Pinto, H. J., Scalo, J., Maciel, W. J., & Flynn, C. 2000, *ApJ*, 531, L115
- Rosswog, S., Davies, M. B., Thielemann, F.-K., & Piran, T. 2000, *A&A*, 360, 171
- Seidov, Z. 1971, *Ast. Zh.*, 48, 443
- Sigurdsson, S., & Rees, M. J. 1997, *MNRAS*, 284, 318
- Shibata, M. 2000, *Progr. Theor. Phys.*, 104, 325 (arXiv:gr-qc/0007049)
- Shibata, M., Baumgarte, T. W., & Shapiro, S. L. 2000, *ApJ*, 542, 453
- Shibata, M., Karino, S., & Eriguchi, Y. 2002, *MNRAS*, 334, L27

- Shibata, M., Karino, S., & Eriguchi, Y. 2003, MNRAS, 343, 619
- Shibata, M., & Karino, S. 2004, Phys. Rev. D, 70, 084022
- Shibata, M., Taniguchi, K., & Uryu, K. 2005, Phys. Rev. D, 71, 084021
- Spallicci, A. 2003, Virgo Technical Notes VIR-NOT-OCA-1390-257, 1 October 2003, 1
- Spallicci, A., Aoudia, S., de Freitas Pacheco, J. A., Regimbau, T., & Frossati, G. 2005, Class. Quantum Grav., 22, 461
- Stergioulas, N. 2003, Living Reviews in Relativity, 6, 3
- Stergioulas, N., & Friedman, J. L. 1998, ApJ 492, 301
- Taylor, J. H., & Weissberg, J. M. 1989, ApJ, 345, 434
- Thorne, K. S., & Campolattaro, A. 1967, ApJ, 149, 591
- Thorne, K. S. 1969, ApJ, 158, 1
- Thorne, K. S. 1980, Rev. Mod. Phys., 52, 299
- Thompson, C., & Duncan, R. C. 1993, ApJ, 408, 194
- Traylor, G., et al. 2007, Phys. Rev. D, 76, 062003
- Tutukov, A. V., & Yungelson, L. R. 1993, MNRAS, 260, 675
- Ushomirsky, G., Cutler, C., & Bildsten, L. 2000, MNRAS, 319, 902
- Vallisneri, M. 2003, in 2001: A Relativistic Spacetime Odyssey, Proceedings of the 25th Johns Hopkins Workshop on Current Problems, eds., Ignazio Ciufolini, Daniele Dominici, & Luca Lusana (New Jersey: World Scientific)(arXiv:gr-qc/0202037)
- Valluri, M., Ferrarese, L., Merritt, D., & Joseph, C. L. 2005, ApJ, 628, 137
- van den Heuvel, E. P. J., & Lorimer, D. R. 1996, MNRAS, 283, L37
- Vincent, S. 2008, PhD Thesis, University of Nice-Sophia Antipolis
- Vincent, S., & de Freitas Pacheco, J. A. 2010, in preparation
- Waas, T., Rho, M., & Weise, W. 1997, Nucl. Phys. A, 617, 449
- Watts, A. L., & Strohmayer, T. E. 2007, Ap&SS, 308, 625
- Weber, J. 1960, Phys. Rev., 117, 306
- Weiss, R. 1971, Quaterly Prog. Report of RLE, MIT, 105, 54
- Wiringa, R., Fiks, V., & Fabrocini, A. 1988, Phys. Rev. C, 38, 1010
- Witten, E. 1984, Phys. Rev. D, 30, 272
- Xu, R. X. 2006, Astropart. Phys., 25, 212
- Yoshida, S., & Eriguchi, Y. 2001, MNRAS, 322, 389
- Zdunik, J. L., Bejger, M., Haensel, P., & Gourgoulhon, E. 2006, A&A, 465, 533
- Zwergner, T., & Muller, E. 1997, A&A, 320, 209